Published May 12, 2003

JCB Article

# Role of *Drosophila* Rab5 during endosomal trafficking at the synapse and evoked neurotransmitter release

**Tanja Wucherpfennig,[1,2] Michaela Wilsch-Bräuninger,[1] and Marcos González-Gaitán[1,2]**

[1]Max-Planck Institut für Molekulare Zellbiologie und Genetik, D-01307 Dresden, Germany
[2]Max-Planck Institut für Biophysikalische Chemie, D-37077 Göttingen, Germany

During constitutive endocytosis, internalized membrane traffics through endosomal compartments. At synapses, endocytosis of vesicular membrane is temporally coupled to action potential–induced exocytosis of synaptic vesicles. Endocytosed membrane may immediately be reused for a new round of neurotransmitter release without trafficking through an endosomal compartment. Using GFP-tagged endosomal markers, we monitored an endosomal compartment in *Drosophila* neuromuscular synapses. We showed that in conditions in which the synaptic vesicles pool is depleted, the endosome is also drastically reduced and only recovers from membrane derived by dynamin-mediated endocytosis. This suggests that membrane exchange takes place between the vesicle pool and the synaptic endosome. We demonstrate that the small GTPase Rab5 is required for endosome integrity in the presynaptic terminal. Impaired Rab5 function affects endo- and exocytosis rates and decreases the evoked neurotransmitter release probability. Conversely, Rab5 overexpression increases the release efficacy. Therefore, the Rab5-dependent trafficking pathway plays an important role for synaptic performance.

## Introduction

At the presynaptic terminal, $Ca^{2+}$-triggered neurotransmitter (NT)* release by exocytosis is immediately followed by the local recycling of the synaptic vesicle (SV) membrane (Ceccarelli et al., 1973; Heuser and Reese, 1973; for reviews see Hannah et al., 1999; Jarousse and Kelly, 2001). SV recycling is necessary to preserve the plasma membrane surface area, to sustain the population of SVs, and to maintain the molecular diversity of the vesicle versus the plasma membrane.

There are at least two distinct recycling mechanisms: "kiss and run" (Ceccarelli et al., 1973; Fesce et al., 1994; Stevens and Williams, 2000) and clathrin-mediated endocytosis (Heuser and Reese, 1973). During kiss and run, SVs make brief contact with the plasma membrane forming a transient porelike structure through which the NT is released (for review see Valtorta et al., 2001). In contrast, clathrin-mediated endocytosis occurs after complete fusion of the SV with the plasma membrane (for reviews see Hannah et al., 1999; Jarousse and Kelly, 2001). New vesicles are subsequently reformed through a complex process initiated by the formation of an invagination at the plasma membrane mediated by clathrin and its adaptors (Heuser and Reese, 1973; Maycox et al., 1992; Takei et al., 1996; González-Gaitán and Jäckle, 1997; Zhang et al., 1998). In lamprey, snake, and fly neuromuscular synapses, the invagination of the membrane into pits occurs at distinct "centers of endocytosis" surrounding the active zones of exocytosis (González-Gaitán and Jäckle, 1997; Ringstad et al., 1999; Roos and Kelly, 1999; Teng and Wilkinson, 2000; Jarousse and Kelly, 2001). Subsequently, amphiphysin, dynamin, and endophilin are thought to lead to the formation of a clathrin-coated, endocytic vesicle (Koenig and Ikeda, 1989; Hinshaw and Schmid, 1995; Takei et al., 1995; Shupliakov et al., 1997; Ringstad et al., 1999; Schmidt et al., 1999). The subsequent steps are still a matter of debate and it is controversial whether endocytic vesicles mature directly into SVs, recycle through an intermediate endosomal compartment before they become SVs, or whether both pathways are used under different conditions of synaptic demand.

In nonneuronal cells, it is well established that endocytic vesicles fuse with endosomes (Helenius et al., 1983) in a process mediated by the small GTPase Rab5 (Bucci et al., 1992; Horiuchi et al., 1997). Through the recruitment of several effector molecules, Rab5 has been suggested to form

Address correspondence to Marcos González-Gaitán, Max-Planck Institute, Pfotenhauerstrasse 108, Dresden, D-01307 Germany. Tel.: 49-551-210-2539. Fax: 49-551-210-1389. E-mail: gonzalez@mpi-cbg.de

*Abbreviations used in this paper: $[Ca^{2+}]e$, external $Ca^{2+}$ concentration; CNS, central nervous system; CSP, cystein string protein; LTR, long terminal repeat; mEJP, miniature excitatory junction potential; NMJ, neuromuscular junction; NT, neurotransmitter; PI(3), phosphatidylinositol-3; PI(3)P, PI(3)-phosphate; PNS, peripheral nervous system; SV, synaptic vesicles.

Key words: neuromuscular junction; FYVE domain; small GTPase; shibire; dynamin

Published May 12, 2003



a specialized membrane domain (Rab5 domain) at the early endosome (Sonnichsen et al., 2000; De Renzis et al., 2002). Based on this, Rab5 has been used as a marker for early endosomes (Bucci et al., 1992; Fialka et al., 1999; Roberts et al., 1999; Sonnichsen et al., 2000). Active Rab5 recruits two phosphatidylinositol-3-kinases (PI[3]-kinases), p85α/p110β and VPS34/p150, which trigger a local enrichment of phosphatidylinositol-3-phosphate (PI[3]P) in the endosomal membrane (Christoforidis et al., 1999). PI(3)P specifically binds to the FYVE zinc-finger domain of endosomal factors such as the Rab5 effectors EEA1 and Rabenosyn-5, which ultimately mediate endocytic vesicle tethering and fusion with the endosome (Stenmark et al., 1995; Simonsen et al., 1998; Lawe et al., 2000; Nielsen et al., 2000). Consistently, blocking the PI(3)-kinases with antibodies or wortmannin impairs the association of FYVE domain proteins with the endosome and, thereby, blocks endosomal trafficking (Mills et al., 1998; Simonsen et al., 1998). Furthermore, it has been shown that the FYVE domain binds to PI(3)P only when inserted in a lipid bilayer (Misra and Hurley, 1999; Sankaran et al., 2001) and that the localization of a myc-tagged tandem repeat of the FYVE domain (myc-2xFYVE) is restricted to early endosomes and the internal membrane of multivesicular bodies (Gillooly et al., 2000). Therefore, 2xFYVE is a bona fide marker for the PI(3)P-containing endosomes.

Rab5 has been found on SVs (de Hoop et al., 1994; Fischer von Mollard et al., 1994), suggesting that SVs have the capacity to fuse with an endosomal compartment. Furthermore, both neuroendocrine PC12 cells (de Wit et al., 1999) and hippocampal neurons (de Hoop et al., 1994) contain synaptic-like vesicles that traffic in a Rab5-dependent manner through endosomal compartments at least in the absence of synaptic transmission. However, it is unclear whether these Rab5-dependent endocytic pathways act only during nourishment and cell signaling in neurons, or also function in the recycling and maturation of SVs during synaptic transmission.

In favor of SV recycling through the endosome, it has recently been suggested that a neuron-specific isoform of the AP3 clathrin adaptor complex from brain cytosol is required for SV budding from PC12 cell endosomes (Faundez et al., 1998; Blumstein et al., 2001). Furthermore, FM1–43 styryl dye recycling experiments in the *Drosophila* neuromuscular junction (NMJ) uncovered two recycling pathways, a rapid and a slower one, suggesting the existence of an endosome-dependent pathway (Koenig and Ikeda, 1996). However, in rat hippocampal neurons in culture, FM1–43 experiments suggested that SVs retain their identity through the endocytic cycle, implying that the SV membrane does not traffic through an intermediate endosome (Murthy and Stevens, 1998). In addition, SV recycling in neurons is likely too rapid to allow for constitutive trafficking through an intermediate endosomal compartment (Pyle et al., 2000; Richards et al., 2000). However, not all vesicles participate in the endo–exo recycling at any given time. Remaining ves-

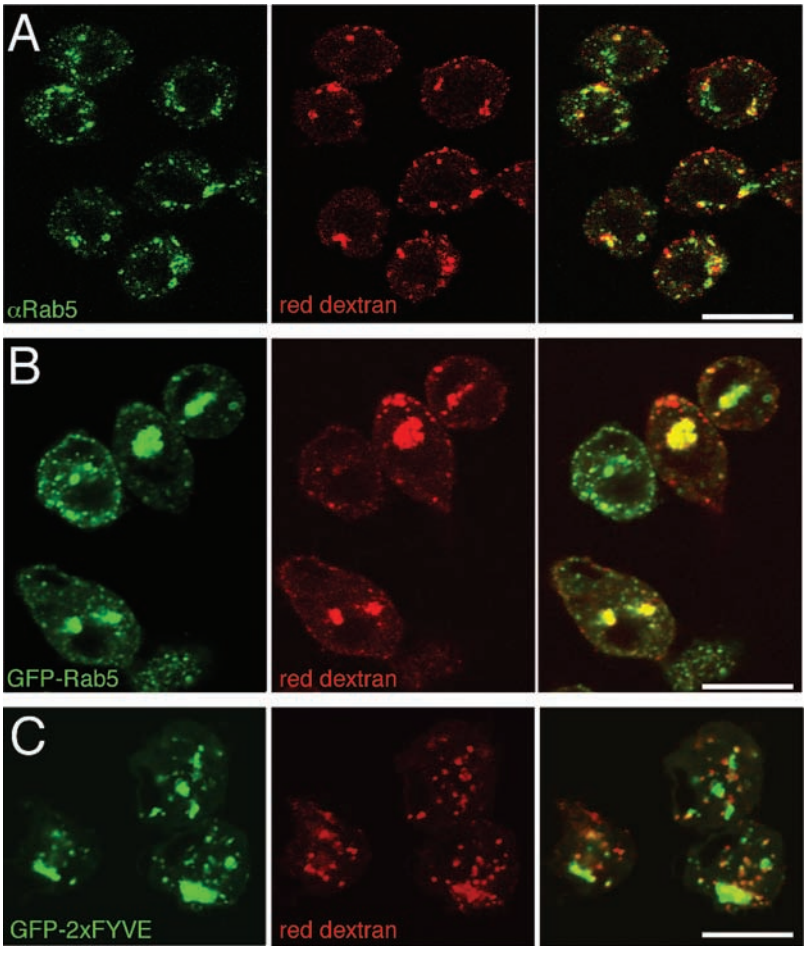


Figure 1. **Rab5 and GFP-2xFYVE are associated to endosomal structures.** Double labelings of *Drosophila* S2 cells showing (A) endogenous Rab5 immunostaining, (B) GFP-Rab5, or (C; left, green) GFP-2xFYVE and (A–C; middle, red) Texas red–dextran internalized upon a 5-min pulse. (Right panels) Overlay. Note that a substantial amount of the endogenous Rab5, GFP-Rab5, or GFP-2xFYVE–positive structures colocalize with the early endosomes where the dextran accumulates upon a short pulse. Bars, 10 μm.

Published May 12, 2003



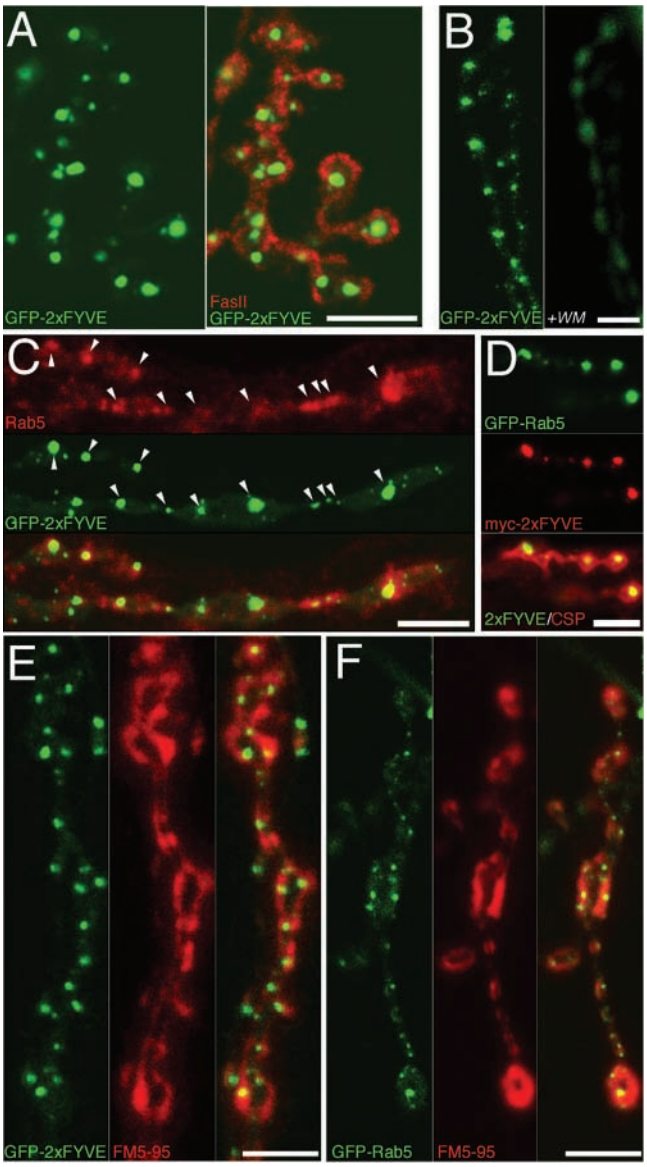


Figure 2. **An endosomal compartment at the presynaptic terminal.** (A) Double labeling showing GFP-2xFYVE (green) to monitor the endosomes and Fasciclin II immunostaining to label the NMJ presynaptic terminals (FasII, red). (B) GFP-2xFYVE fluorescence in an abdominal muscles 6/7 NMJ before (left) and after (right) a 45-min treatment with 100 nM wortmannin in vivo. Note that, upon wortmannin treatment, GFP-2xFYVE looses the punctate pattern and becomes dispersed into the cytosol. Untreated controls retained the punctate pattern (see Materials and methods). (C) Double labeling showing endogenous Rab5 immunostaining (red) and GFP-2xFYVE (green); lower panel shows merge. Arrowheads indicate Rab5 punctate structures colocalizing with GFP-2xFYVE–positive endosomes. Notice also that some of the Rab5 endosomes do not contain GFP-2xFYVE, consistent with two types of Rab5 endosomes, EEA1 positive/negative, as described previously (Wilson et al., 2000). (D) Triple labeling showing GFP-Rab5 (top, green), endosomal myc-2xFYVE immunostaining using an anti–c-myc antibody (middle, red; bottom, green) and CSP immunostaining (CSP, bottom, red) to label the presynaptic terminals in a muscles 6/7 NMJ. Bottom panel is a merge of myc-2xFYVE and CSP. GFP-Rab5 and myc-2xFYVE show a complete colocalization. Double labelings in green (E) GFP-2xFYVE or (F) GFP-Rab5 and in red FM5–95 styryl dye internalized into the presynaptic terminal upon a 1-min stimulation with 60 mM $K^+$ to label the pool of recycling vesicles (E and F) in two different abdominal muscles 6/7 NMJs. Right panels show merge. Note that the endosomes are embedded within the pool of recycling vesicles. Genotypes: (A–C and E) *w; UAS-GFP-myc-2xFYVE; elav-GAL4*; (D) *w; UAS-myc-2xFYVE/elav-GAL4 UAS-GFP-Rab5*; and (F) *w; elav-GAL4/UAS-GFP-Rab5*. Bars, 5 μm. In this and the following figures, NMJs from late third instar larvae are shown unless otherwise indicated.

icles may have sufficient time to exchange membrane with the endosome.

Here, we use the *Drosophila* larval NMJ as a model system to study the endosomal pathway at the presynaptic terminal for synaptic function.

## Results

### An endosomal compartment in the presynaptic terminal

Both Rab5 and myc-2xFYVE have been used as endosomal markers in cultured nonneuronal mammalian cells (Bucci et al., 1992; Gillooly et al., 2000). To monitor the endosomes, we generated GFP-2xFYVE, myc-2xFYVE, and GFP-Rab5 fusions and produced a specific anti-*Drosophila* Rab5 (anti-DRab5) antibody (see Materials and methods). Endogenous Rab5 as well as the GFP-Rab5 and the GFP-2xFYVE fusions are localized at the endosome, as monitored by Texas red–dextran internalization experiments in *Drosophila* S2–cultured cells (Fig. 1) and developing wing cells (unpublished data). Using the UAS/GAL4 technique in transgenic flies (Brand and Perrimon, 1993), we specifically expressed the tagged 2xFYVE fusions in the central nervous system (CNS) with elav-GAL4. Both GFP-2xFYVE and myc-2xFYVE–labeled endosomes appeared as punctate structures at the presynaptic terminal of third instar larval NMJs (Fig. 2 A; unpublished data). At least one 2xFYVE-labeled endosome was detected per presynaptic terminal (Fig. 2, A and E). As in cultured mammalian cells, 2xFYVE becomes dispersed into the cytosol upon blockage of PI(3)-kinase activity using wortmannin (Fig. 2 B), consistent with its PI(3)P-dependent localization at the endosome (Gillooly et al., 2000).

Using the anti-DRab5 antibody, we also found endogenous Rab5 enriched in punctate structures at the presynaptic terminal (Fig. 2 C). In addition, diffused Rab5 was found at lower levels (Fig. 2 C), which likely corresponds to Rab5 present in the cytosol and on vesicles as seen in mammalian cells (Chavrier et al., 1990; Bucci et al., 1992). No overt plasma membrane staining could be detected in a double immunostaining with anti-HRP antibodies (Sun and Salvaterra, 1995; unpublished data). A substantial amount of Rab5 structures colocalize with the GFP-2xFYVE endosomes, indicating that the Rab5 compartment corresponds to the PI(3)P containing endosome (Fig. 2 C). This was confirmed by the colocalization of a functional GFP-Rab5 fusion (see below) and myc-2xFYVE in transgenic flies coexpressing both markers in the CNS (Fig. 2 D).

Next, we compared the localization of the endosomal compartment with the pool of recycling vesicles. EM studies have shown that, in *Drosophila* NMJs, the SV pool does not occupy the entire synaptic bouton (Atwood et al., 1993; Jia et al., 1993). Light microscopy has also been used to demon-

Published May 12, 2003



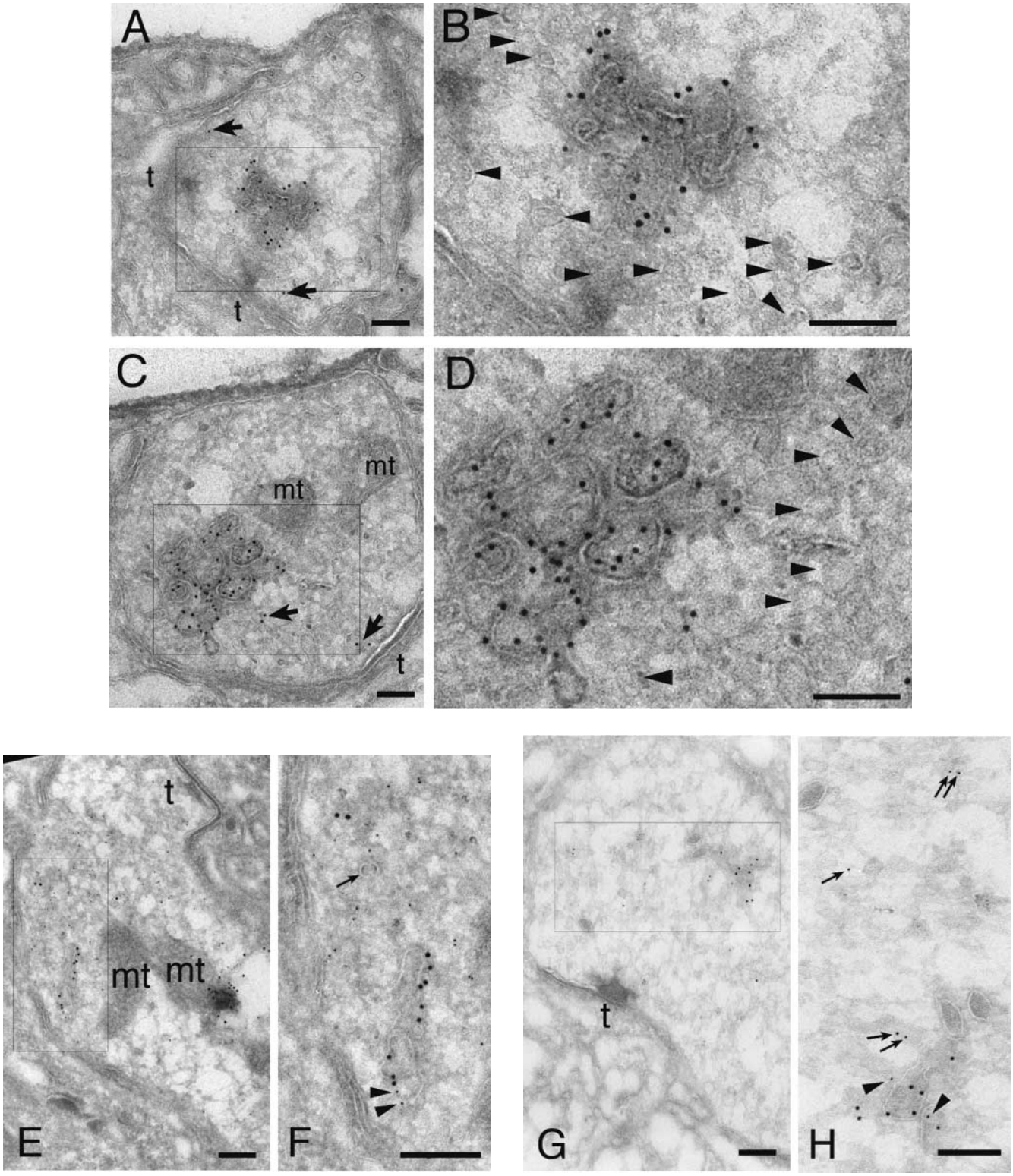


Figure 3. **Cryoimmuno-EM of the GFP-2xFYVE endosome.** (A–D) Cryoimmuno-electron micrographs showing two *Drosophila* presynaptic terminals (A/B and C/D), where GFP-2xFYVE is labeled by 10-nm gold particles (anti-GFP antibody). (B and D) High magnifications of the boxes in A and C, respectively. We found cisternal structures of around 150 nm associated to a more electron-dense region within the terminal. The darker regions allow a better contrast for visualization of the membrane (which appear lighter in cryosections) associated to the endosomes, compared with the vesicles with a diameter of ~35 or 70 nm (see also Fig. 7). Vesicles are, however, occasionally observed (arrowheads). Only few gold particles (7.8 ± 1.3%, $n = 5$ sections) are associated to the vesicles (arrows). Cryoimmuno-electron micrographs showing localization of GFP-2xFYVE (10-nm gold particles) and endogenous CSP (5 nm gold; E and F) or endogenous Rab5 (5 nm gold; G and H). (F and H) High magnifications of the boxes in E and G, respectively. (E and F) CSP appears throughout the bouton area associated to the pool of vesicles, whereas GFP-2xFYVE is largely restricted to the cisternal endosomal compartments. Although not many vesicles are distinguishable (F, arrow), their presence is revealed by staining of SV integral membrane protein CSP. Few 5-nm gold particles labeling CSP could also be

Published May 12, 2003



strate that the SV pool defines a subdomain within the synaptic boutons (Estes et al., 1996). We labeled the pool of recycling vesicles with the red FM5–95 styryl dye internalized during a 30-Hz or high $K^+$ stimulation protocol (Kuromi and Kidokoro, 2002). The endosomes monitored with GFP-2xFYVE (Fig. 2 E) or GFP-Rab5 (Fig. 2 F) are embedded within the pool of recycling vesicles, indicating that the endosomal compartments are associated to the bouton subdomains where the recycling vesicles are.

Do the GFP-2xFYVE–positive structures correspond to a cisternal endosomal compartment as in the case in cultured mammalian cells (Gillooly et al., 2000) or to a cluster of vesicles within the SV pool? To address this, we performed cryoimmuno-EM and visualized the localization of GFP-2xFYVE in the presynaptic terminal at the ultrastructural level. Fig. 3 shows that, like in mammalian cells (Gillooly et al., 2000), the GFP-2xFYVE structures correspond to cisternal compartments larger than 150 nm and not to a subpopulation of vesicles (35 or 70 nm diam; see Fig. 7) clustered within the SV pool. Thus, >90% of the gold particles (92.2% ± 1.3, $n = 5$ sections with 189 gold particles) are associated to cisternal structures. In cryosections, membranes appear as light lines, which contrast against the more electron-dense cytosolic region associated to the cisternae (Fig. 3). Although vesicle membrane is more difficult to observe (Fig. 3, B and D [arrowheads], and F [arrow]), because vesicles are located in lighter regions of the cytosol, their presence could be detected using an antibody against cystein string protein (CSP), an SV integral membrane protein (Fig. 3, E and F). CSP was also localized at the cisternal structures, consistent with the membrane exchange between the vesicles and the cisternal compartment. This indicates that the GFP-2xFYVE label in the presynaptic terminal (Fig. 2) corresponds to endosomal structures rather than to a cluster of vesicles within the SV pool.

Like GFP-2xFYVE, Rab5 is also associated to the cisternal endosomal structures (Fig. 3, G and H, arrowheads). In contrast to GFP-2xFYVE, which is restricted to the cisternal structures in cultured mammalian cells (Gillooly et al., 2000) and *Drosophila* NMJs (Fig. 3), Rab5 was also found outside the cisterna, associated with the SVs and the cytosol (Fig. 3, G and H, arrows), as described previously (Chavrier et al., 1990; Bucci et al., 1992).

In summary, the light- and electron-microscopical analysis shows that the GFP-2xFYVE–positive structures at the presynaptic terminal correspond to endosomal structures, where Rab5 is enriched, and that they are located within the pool of SVs.

## Endosomal dynamics during synaptic transmission

Next, we analyzed the behavior of the endosome during synaptic transmission by imaging in vivo GFP-2xFYVE during electrophysiological stimulation of the presynaptic terminals (Fig. 4, A–P). In resting terminals or under conditions of basal or tetanic stimulation, we observed no change in location, size, or fluorescence intensity of the GFP-2xFYVE–labeled endosomes (Fig. 4, D and J–L; unpublished data). This is consistent with three possible scenarios: (1) SVs bypass the endosome; (2) vesicle membrane fusion to and budding from the endosome are in balance both in the resting terminal and during synaptic transmission; or (3) both pathways operate in parallel.

To address these possibilities, we studied the endosomal dynamics in experimental conditions in which we deplete the SV pool. If membrane exchange between the vesicle pool and the endosome occurs, depletion of the vesicle pool should ultimately result in reduction of the endosomal size. At the *Drosophila* larval NMJ, endocytosis is tightly coupled to synaptic transmission and NT release. In the absence of SV exocytosis, basal endocytosis was not detectable (Ramaswami et al., 1994), and the membrane internalized during synaptic transmission is incorporated into SVs because most of the endocytosed vesicles are releasable (Kuromi and Kidokoro, 2000). We caused a reversible SV depletion by performing a "*shi*$^{ts}$/depletion" experiment by blocking endocytosis using the thermosensitive dynamin mutation *shibire*$^{ts1}$ (*shi*$^{ts}$) at the restrictive temperature (Koenig and Ikeda, 1989; Koenig and Ikeda, 1999) while continuously stimulating SV release. Next, we monitored the GFP-2xFYVE–labeled endosomes after 5, 10, and 15 min of electrophysiological tetanic stimulation at 30 Hz. Fig. 4 (A–D) shows that the endosomal staining disappeared during the *shi*$^{ts}$/depletion experiment. No change was observed in *shi*$^{ts}$ synapses at the permissive temperature (unpublished data). The endosomal depletion does not depend on the stimulation being tetanic because GFP-2xFYVE endosomal staining also disappears under stimulation at 3 Hz (Fig. 4, E–G). The kinetics of fluorescence decay at the endosomes depends on the frequency of stimulation with $t_{1/2}$ of 5 min during basal stimulation at 3 Hz (Fig. 4, D–G) and approximately 10-fold faster during tetanic stimulation at 30 Hz (Fig. 4, A–C).

Dynamin-dependent disappearance of the GFP-2xFYVE endosomal staining can be explained in two ways: either the endosome is depleted due to the depletion of the pool of vesicles in the endocytosis-defective *shi*$^{ts}$ terminal, or association of GFP-2xFYVE to the endosome is dynamin dependent. The observation that no change of the GFP-2xFYVE endosomal staining was detectable in *shi*$^{ts}$ presynaptic terminals at the restrictive temperature when the terminal was not stimulated (unpublished data), makes rather implausible that association of GFP-2xFYVE to the endosome is dynamin independent, unless the GFP-2xFYVE association to the endosome depends on dynamin only during synaptic transmission. Therefore, these results suggest that there is membrane exchange between the vesicle pool and the endosome, so that when the SV pool

observed in the cisternal structures (F, arrowheads). Rab5 appears in the cisternal structures, (H, arrowheads) as well as in other regions corresponding to vesicles or cytosol (H, arrows). Note that immunodetection is highly specific, because neither 10-nm (GFP-2xFYVE) or 5-nm gold particles (CSP and Rab5) were very rarely detected in the postsynaptic subsynaptic reticulum or the mitochondria in the cryosections (<1% of the gold particles; A–H; unpublished data). t, T-bar or electron-dense regions indicating active zones; mt, mitochondria. Bars: (A–D) 150 nm; (E–H) 200 nm.

Published May 12, 2003



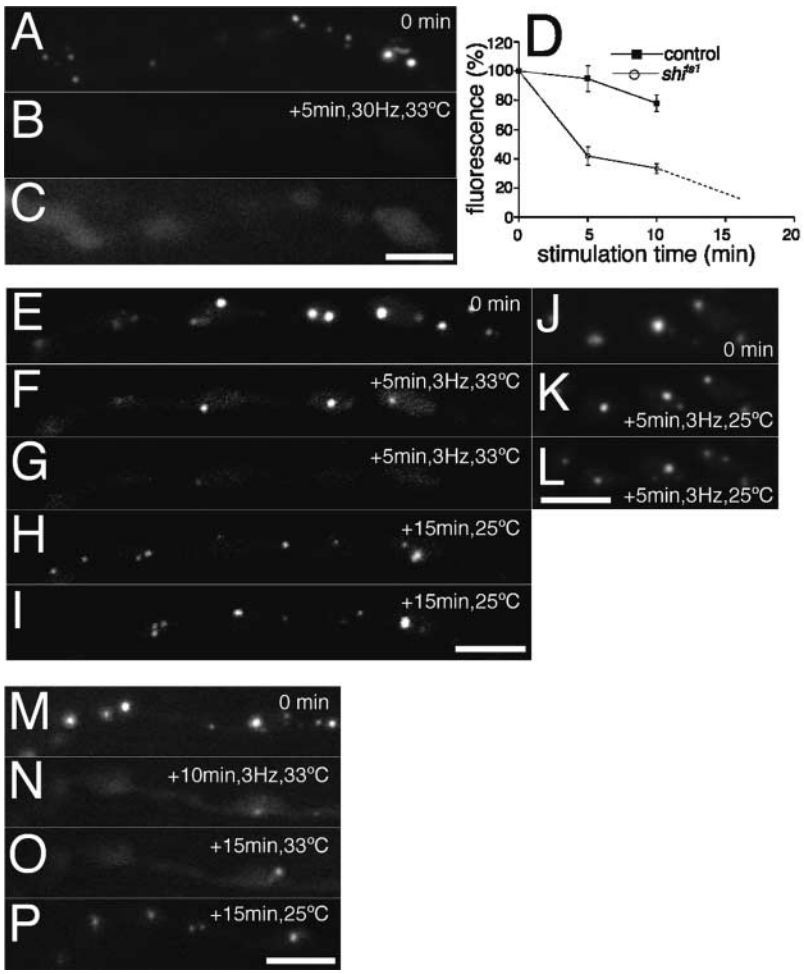


Figure 4. **Membrane exchange between vesicles and the synaptic endosome.** GFP-2xFYVE labeling in a (A) *shi*$^{ts}$ mutant terminal at 25°C and (B and C) after 5 min of stimulation (30 Hz, normal saline) at 33°C. Genotype: *shi*$^{ts}$; elav-GAL4 UAS-GFP-myc-2xFYVE. (C) Same image as in B, with increased contrast and brightness to show diffused GFP-2xFYVE fluorescence at the terminal. The endosome is drastically reduced together with the pool of vesicles in *shi*$^{ts}$ terminals. No change was observed in resting or stimulated control NMJs or in *shi*$^{ts}$ at 25°C. The endosomes remained also normal in resting *shi*$^{ts}$ NMJs at 33°C. (D) Kinetics of disappearance of the endosome. Time course of the changes in GFP-2xFYVE fluorescence in *shi*$^{ts}$; *elav-GAL4 UAS-GFP-myc-2xFYVE* (*shi*$^{ts}$; $n = 5$ NMJs) and *w; elav-GAL4 UAS-GFP-myc-2xFYVE* (control; $n = 4$ NMJs) during 3 Hz at 33°C. Fluorescence in ordinates refers to mean pixel brightness at the punctate structures normalized to the mean brightness before stimulation. After 20 min of stimulation at 33°C in *shi*$^{ts}$ (dashed line), GFP-2xFYVE fluorescence at the endosome cannot be distinguished. (E) GFP-2xFYVE labeling in a *shi*$^{ts}$ mutant terminal at 25°C and (F) after stimulation at 33°C for 5 and (G) 10 min at 3 Hz. (H and I) GFP-2xFYVE fluorescence recovery at the endosomes in the same synapses upon downshift to 25°C for (H) 15 and (I) 30 min. Genotype in E–I: *shi*$^{ts}$; *elav-GAL4 UAS-GFP-myc-2xFYVE*. Fluorescence is recovered after releasing the endocytosis block, suggesting that the endosome recovers from membrane derived by dynamin-mediated endocytosis. (J–L) Control: *w; elav-GAL4 UAS-GFP-myc-2xFYVE* synapses showing GFP-2xFYVE fluorescence upon a 3-Hz stimulation during the same time intervals (J, 0 min; K, 5 min; L, 10 min) at 25°C. (M) GFP-2xFYVE labeling in a *shi*$^{ts1}$ mutant terminal at 25°C and (N) after stimulation at 33°C during 10 min at 3 Hz. (O) GFP-2xFYVE fluorescence in the same synapses maintained at 33°C for 15 min after stimulation followed by (P) downshift to 25°C for 15 min. In the resting terminal, fluorescence is recovered at the endosome only if the endocytosis block is released, indicating that endosomal recovery occurs at the expense of newly formed endocytic vesicles. In A–P NMJs belong to A2–A4 abdominal muscles 6/7. Bars, 5 μm. In this and the following figures the error bars are standard errors.

is depleted in endocytosis-defective terminals, the endosome is subsequently reduced or even depleted.

Consistent with this idea, the endosome is recovered only when the endocytic block is released. We first depleted the endosome by performing a *shi*$^{ts}$/depletion experiment as described above (Fig. 4, E–G). Animals were then returned to the permissive temperature to release the *shi*$^{ts}$ block. After 15 min, we observed recovery of the GFP-2xFYVE–labeled endosome (Fig. 4, H and I). Furthermore, if we first depleted the endosome as described above (Fig. 4, M and N) and then maintained the animals at the restrictive temperature after stimulation, no endosomal recovery was observed (Fig. 4 O). Returning the animals to the permissive temperature to release the endocytosis block, led to the recovery of the endosome (Fig. 4 P). Therefore, endosomal recovery only occurs after release of the endocytosis block suggesting that newly formed endocytic vesicles replenish the endosomal compartment.

Together, these results suggest that the endosomal compartment is replenished by vesicles derived by dynamin-dependent endocytosis that fuse to the endosome and that endosomal membrane can be converted into SV membrane at least under our experimental conditions. This suggests that a trafficking pathway exists, which may not be obligatory, involving the endosome during SV recycling.

## Rab5 mutants show locomotion defects, paralytic phenotypes, and defective endosomes

In *Drosophila*, we found a single Rab5 gene with multiple splicing variants coding for a single ORF (Fig. 5 A; see Materials and methods). Consistently, we detected a single 24-kD band in Western blot experiments using the anti-*Drosophila* Rab5 antibody against embryonic or larval extracts (unpublished data). This is in contrast to the situation in yeast and mammalian cells where three Rab5 genes coding for different isoforms were found (Novick and Zerial, 1997), whereas in *Caenorhabditis elegans* a single Rab5 gene was found (Grant and Hirsh, 1999).

We identified two P-elements from the Berkeley genome project inserted in the Rab5 gene (Fig. 5 A), *P{lacw}Rab5-k08232* and *P(PZ+)00231*. *P{lacw}Rab5k08232* (*Rab5*$^{1}$) is a P-element insertion within the 5′ leader coding region (Fig. 5 A). Homozygous mutants expressed 30% of the wild-type Rab5 protein level as estimated in Western blot

Published May 12, 2003



experiments with larval extracts (unpublished data; see Materials and methods). Homozygous *Rab5[1]* animals die during late second and early third instar larval stages with only a light locomotion phenotype. Consistent with a mild phenotype, in *Rab5[1]* both the FM1–43 uptake rates and synaptic transmission monitored by standard electrophysiological recordings of the evoked junctional potential in the mutant muscles are normal (unpublished data; see Materials and methods). The *Rab5[1]* lethality and phenotype are caused by reduced Rab5 levels in the nervous system because they could be rescued by restricted expression of GFP-Rab5 in the nervous system using elav-GAL4. This also indicates that GFP-Rab5 is a functional Rab5 fusion and that Rab5 function is essential during the physiology and/or development of the nervous system. Consistently, two other weaker Rab5 alleles, *Rab5[3]* and *Rab5[4]* (Fig. 5 A; see Materials and methods), lead to a flightless phenotype in homozygous adult flies.

A more severe mutation, *Rab5[2]*, causes embryonic lethality with a paralytic phenotype. *Rab5[2]* is a 4-kb deletion of the promotor region, the 5′ nontranslated leader and the first exon of the ORF (Fig. 5 A). This exon encodes the PM1–3 phosphate/$Mg^{2+}$-binding motifs and the G1 guanine base-binding motif of the GTPase domain (Olkkonen and Stenmark, 1997). Therefore, *Rab5[2]* is likely a Rab5-null mutation. Western blot experiments with *Rab5[2]* homozygous mutant embryos (0–22 h) showed a faint Rab5 band (13% of the wild-type level; unpublished data), which corresponds to maternal Rab5. Consistent with a maternal Rab5 contribution, the Rab5 protein was also detected by Western blot experiments in early embryonic stages (0–2 h), when most proteins derive from maternal mRNAs (unpublished data). This implies that the zygotic loss of Rab5 is partially rescued by the maternal Rab5 contribution. Like in the case of other endocytic mutants, such as dynamin (Swanson and Poodry, 1981) and α-adaptin (unpublished data), loss of maternal Rab5 contribution in germ line clones impairs cellularization and leads to an early embryonic arrest, so that no nervous system is formed (unpublished data).

Zygotic loss of Rab5 caused the disruption of the GFP-2xFYVE endosomes in the embryonic nervous system (Fig. 5, B–E). In control embryos the endosomes appeared as punctate structures within the cell bodies of the CNS (Fig. 5 B) and the peripheral nervous system (PNS; Fig. 5 C) as monitored with GFP-2xFYVE driven by elav-GAL4. Like in larval stages, the NMJ of late control embryos (stage 17) displayed GFP-2xFYVE–positive endosomal punctate structures within the presynaptic terminals (Fig. 5 D). In contrast, GFP-2xFYVE was dispersed in the cytosol in the *Rab5[2]* mutant embryonic CNS, including the NMJs and the PNS (Fig. 5, B, C, and E). In summary, these data indicate that Rab5 is required for the integrity of the endosome during embryonic development and for the development and/or function of the nervous system.

## Ultrastructural analysis presynaptic terminals with impaired Rab5 function

The Rab5 mutants described above represent a deficit of Rab5 function both at the presynaptic (neuron) and

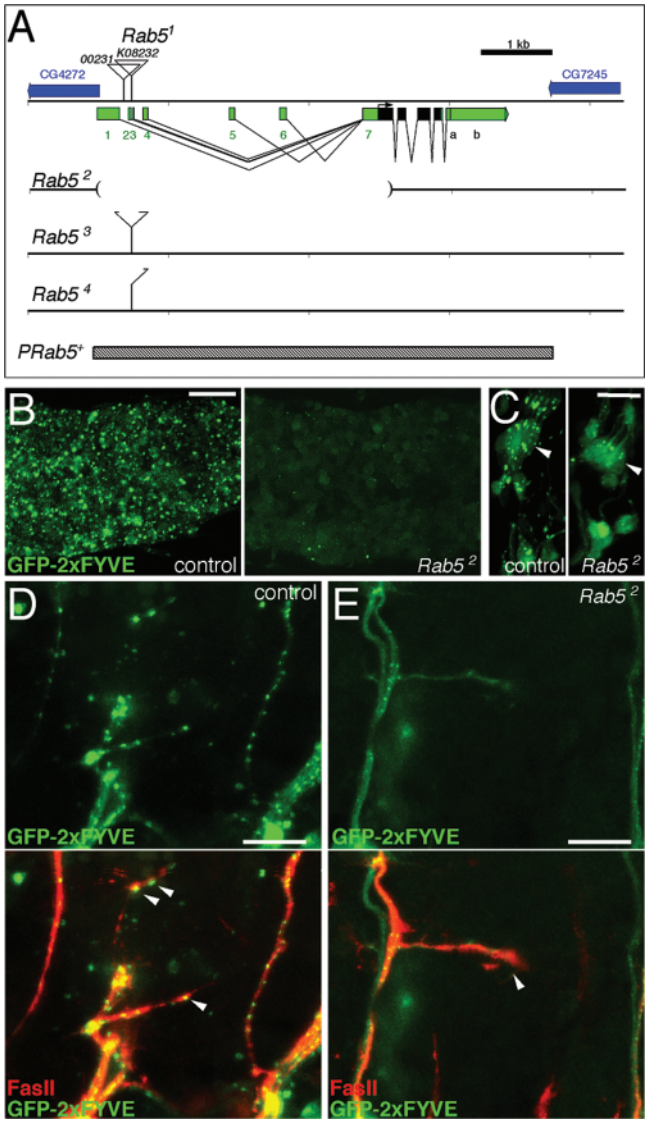


Figure 5. ***Rab5* loss of function mutants show disrupted endosomes.** (A) *Rab5* genomic organization. (Green/black bars) Rab5 exons. (1–7) Alternative 5′ leader exons. (a and b) Alternative 3′ untranslated regions. (Black bars) ORF. (Blue arrows) Rab5 flanking genes (CG4272 and CG7245). (*00231* and *K08232)* P-element insertions. We renamed *l(2)K08232* as *Rab5[1]*. (*Rab5[2]*) 4-kb deletion generated by imprecise excision of *Rab5[1]*. *Rab5[3]* and *Rab5[4]* are imprecise excisions where P-element LTR sequences remained (see Materials and methods). *PRab5[+]* (hatched bar), region contained in the genomic *Rab5* rescue. (B) GFP-2xFYVE labeling in the CNS of control (left, genotype: *w; elav-GAL4 UAS-GFP-myc-2xFYVE*) and *Rab5[2]* mutant embryos stage 17 (right, *Rab5[2]; elav-GAL4 UAS-GFP-myc-2xFYVE*). Note, in the control, the punctate appearance of endosomes labeled by GFP-2xFYVE in the soma of the CNS and in *Rab5[2]* mutant embryos the diffuse GFP-2xFYVE fluorescence dispersed in the cytosol, indicating that the endosome is severely affected. (C) GFP-2xFYVE labeling in the PNS of control (left) and *Rab5[2]* embryos (right). Genotypes as in B. (Arrowheads) Pentachordotonal sensory neurons. (D and E) Double labeling showing the GFP-2xFYVE marked endosomes (green) and Fasciclin II immunostainings (red) to monitor the motoneurons at the NMJ (arrowheads) of control (D) and *Rab5[2]* embryos (E). Lower panels, merges of the two channels. Genotypes as in B. Note that few remnant GFP-2xFYVE punctate structures can be observed occasionally in the *Rab5[2]* mutant embryos, probably due to rescue by the Rab5 maternal contribution. Bars: (B) 20 μm; (C–E) 10 μm.

Published May 12, 2003



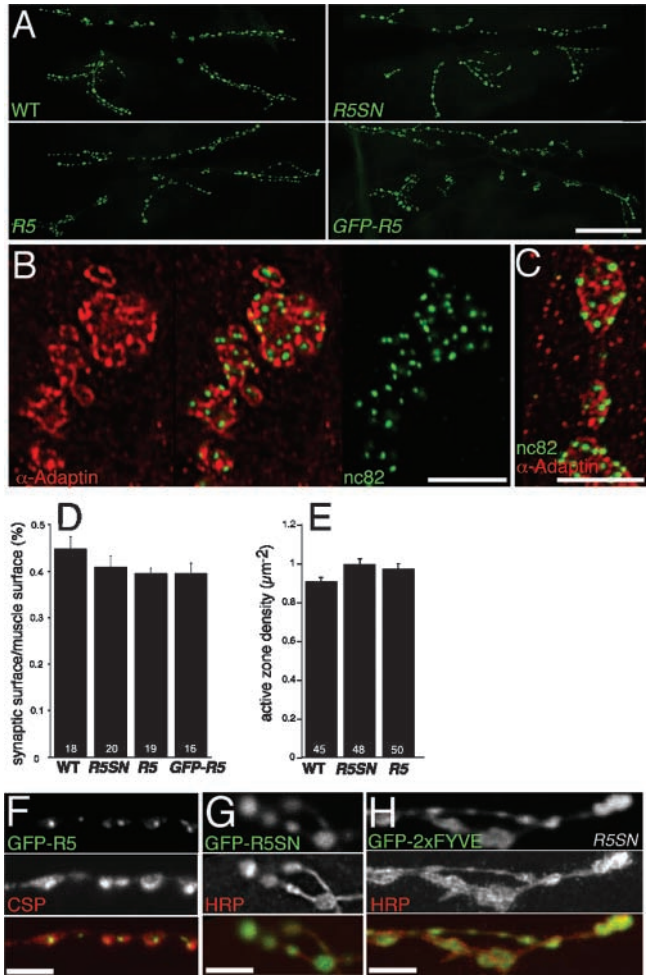


Figure 6. **Normal synaptic morphology and disrupted endosomes in mutant Rab5 expressing presynaptic terminals.** (A) CSP immunolabeling of muscles 6/7 NMJs in the A2 segment of wild-type (WT), *w; UAS-Rab5S43N/+; elav-GAL4/+* (*R5SN*), *w; UAS-Rab5/+; elav-GAL4/+* (*R5*), and *w; elav-GAL4/UAS-GFP-Rab5* (GFP-*R5*) larvae. (B and C) Double immunostaining showing the centers of endocytosis labeled with α-adaptin (red) and the active zones of exocytosis labeled with nc82 antibodies (green) in a (B) wild-type and a (C) *w; UAS-Rab5S43N/+; elav-GAL4/+* presynaptic terminal. In B, middle panel is the merge. (D) Mean synaptic surface area and (E) mean active zone density in muscles 6/7 of A2 in wild-type and different mutants. Active zone density is the number of nc82 active zones per terminal area. Genotypes as in A. Numbers in the columns are the number of NMJs (D) and presynaptic terminals quantified (E). Neither the synaptic area nor the active zone density is significantly different in the mutants, implying that the total number of active zones is normal in the mutants. (F) Double labeling showing GFP-Rab5 and CSP immunostaining to monitor the presynaptic terminal in a *w; UAS-GFP-Rab5/elav-GAL4* NMJ. (Bottom panel) Merge of the GFP-Rab5 (green) and CSP (red) stainings. Note the punctate staining of GFP-Rab5 associated to the endosomes. (G) Double labeling showing GFP-Rab5S43N and HRP immunostaining to monitor the NMJ in a *w; UAS-GFP-Rab5S43N/+; elav-GAL4/+* NMJ. (Bottom panel) Merge of the GFP-Rab5S43N (green) and HRP (red) stainings. GFP-Rab5S43N is not associated to endosomes and appears dispersed in the cytosol of the presynaptic terminal. (H) Double labeling showing GFP-2xFYVE to label the endosomes and HRP immunostaining to monitor the presynaptic terminal in a *w; UAS-GFP-myc-2xFYVE; elav-GAL4/UAS-Rab5S43N* NMJ. (Bottom panel) Merge of the GFP-2xFYVE (green) and HRP (red) stainings. The GFP-2xFYVE endosomal compartment is disrupted upon expression of the dominant-negative Rab5S43N mutant as indicated by the cytosolic GFP-2xFYVE appearance. Bars: (A) 50 μm; (B, C, and F–H) 5 μm. In this and the following figures, when wild-type or mutant Rab5 was expressed using the UAS/GAL4 system, embryonic and early larval development took place at 16°C and animals were shifted to 25°C only during the last 2 d of larval development. When 29°C is indicated, the last 2 d were at this temperature. The controls were submitted to the same procedure.

postsynaptic (muscle) side of the NMJ. To study the specific presynaptic role of Rab5, we expressed a dominant-negative, GDP-bound Rab5 mutant (Rab5S43N; Stenmark et al., 1994; Entchev et al., 2000) exclusively in the nervous system using the UAS/GAL4 technique. To ensure a normal neural development and to study, thereby, the specific mutant effect during synaptic physiology, we capitalized on the thermosensitivity of GAL4 in *Drosophila* (Brand et al., 1996; Entchev et al., 2000). We expressed Rab5S43N at low levels during embryonic and early larval stages at 16°C and at higher levels at 25°C during the last two days of larval development (see Materials and methods).

Fig. 6 (A–E) shows that mutant Rab5S43N expressed this way at the presynaptic terminal did not cause a developmental phenotype of the NMJ. The synaptic surface area was normal in Rab5S43N-expressing synapses (Fig. 6, A and D). In addition, Rab5S43N-expressing motoneurons showed a normal number and morphology of the centers of endocytosis and active zones of exocytosis as visualized by anti–α-adaptin, anti-dynamin (González-Gaitán and Jäckle, 1997; Roos and Kelly, 1999), and nc82 antibodies (Heimbeck et al., 1999), respectively (Fig. 6, B, C, and E; unpublished data). The nc82 antibody recognized an antigen associated to the active zones as monitored by the postsynaptic localization of the glutamate receptors at the active zones (unpublished data) and the pattern of the centers of endocytosis around the active zones (Fig. 6, B and C). This indicates that the development and morphology of the NMJ was normal in Rab5S43N-expressing motoneurons. We next studied the ultrastructure of presynaptic terminals in Rab5 mutants.

The dominant-negative, GDP-bound Rab5 mutant impairs the fusion of endocytic vesicles with the endosome in cultured mammalian cells (Bucci et al., 1992). In mutant Rab5 expressing cultured cells, endocytic vesicles accumulate and the endosomes fragment (Bucci et al., 1992). Therefore, endosomal markers appeared diffuse in the cytosol instead of being accumulated at the endosome as a punctate pattern under these conditions (Bucci et al., 1992). Furthermore, the dominant-negative, GDP-bound mutant of Rab5 is localized to the cytosol (Bucci et al., 1992).

When we expressed the Rab5S43N mutant protein, Rab5 showed a diffuse staining, filling the whole presynaptic terminal of the larval NMJ and did not appear in a punctate pattern (Fig. 6, compare F with G). This indicates that the GDP-bound mutant form of Rab5 is largely in the cytosol and not associated to the endosomal compartment at the synapse. Furthermore, if Rab5S43N was coexpressed with GFP-2xFYVE or GFP-Rab5 to monitor the endosomes in the nervous system, we observed a diffuse GFP localization at the terminal, suggesting that endosomes are severely affected

Published May 12, 2003



(Fig. 6 H; unpublished data). Therefore, Rab5 function is required for the integrity of the endosomal compartment.

We then analyzed these defects at the ultrastructural level. In wild-type presynaptic terminals, we could distinguish two types of vesicles that have been previously reported (Kosaka and Ikeda, 1983; Fergestad et al., 1999): SVs with a diameter of 35 nm (35.9 ± 0.11 nm, $n$ = 1991 vesicles; Fig. 7 A) and a second type of vesicles with a diameter of 70 nm (73.6 ± 2.5 nm, $n$ = 36 vesicles; Fig. 7 A, arrowheads), which have been previously suggested to correspond to recycling intermediates (Kosaka and Ikeda, 1983; Fergestad et al., 1999). In *shi*$^{ts}$ mutants, early stages of endocytosis are blocked, causing the accumulation of nascent endocytic vesicles in the form of collared pits at the plasma membrane. Because the 70-nm vesicles have a very similar diameter to these collared pits (Kosaka and Ikeda, 1983) they could represent newly formed endocytic vesicles. In addition, they are probably transient structures because only 2.1 ± 0.5 ($n$ = 26 sections) were observed in each EM section. As described previously (Koenig et al., 1993), we also observed bigger cisternal and tubular structures of around 150 nm (Fig. 7, B–D) that resemble the GFP-2xFYVE containing endosomes observed by cryoimmuno-EM (Fig. 3).

In *Rab5S43N* synapses, the 70-nm vesicles (70.6 ± 1.1 nm, $n$ = 148 vesicles) were more frequently observed than in wild-type synapses (5.9 ± 1.2, $n$ = 25 sections; Fig. 7 E, arrowheads). Consistent with the *Rab5SN* phenotype reported in cultured mammalian cells, where endocytic vesicles accumulate due to their inability to fuse efficiently with the early endosome (Bucci et al., 1992), this result supports the previous proposal suggesting that the 70-nm vesicles correspond to endocytic intermediates that accumulate in the mutant synapses (Kosaka and Ikeda, 1983; Fergestad et al., 1999).

## Impaired endocytosis and release in Rab5S43N-expressing presynaptic terminals

To study the role of Rab5 during the SV cycle, we monitored endocytosis and recycling as well as the SV pool size by performing FM1–43 internalization and release experiments (Betz and Bewick, 1992). The rate of internalization was assayed by monitoring FM1–43 uptake during a 3-Hz train of stimulation for 3, 5, and 10 min (adapted after a protocol established previously by Kuromi and Kidokoro, 2000; Fig. 8, A–C). In wild-type synapses, FM1–43 fluorescence increased rapidly during the first 3 min of stimulation at 3 Hz (Fig. 8 C). As reported previously, after the first 3 min, the rate of fluorescence uptake was slowed down because part of the internalized dye starts now to be released (Betz and Bewick, 1992, 1993; Ryan and Smith, 1995; Kuromi and Kidokoro, 2000). Therefore, we estimated the rates of internalization by fluorescence uptake during the first 3 min. In Rab5S43N-expressing presynaptic terminals, the rate of FM1–43 internalization was 2.5-fold slower than in wild type (Fig. 8, B and C). This result indicates that endocytosis is reduced when Rab5 function is impaired.

We then studied the kinetics of FM1–43 release in the mutant synapses. First, we loaded the terminal by stimulating the synapse at 30 Hz for 3 min. Under these conditions, the pool of recycling vesicles is saturated with FM1–43 both in wild-type and *Rab5S43N* mutant presynaptic terminals

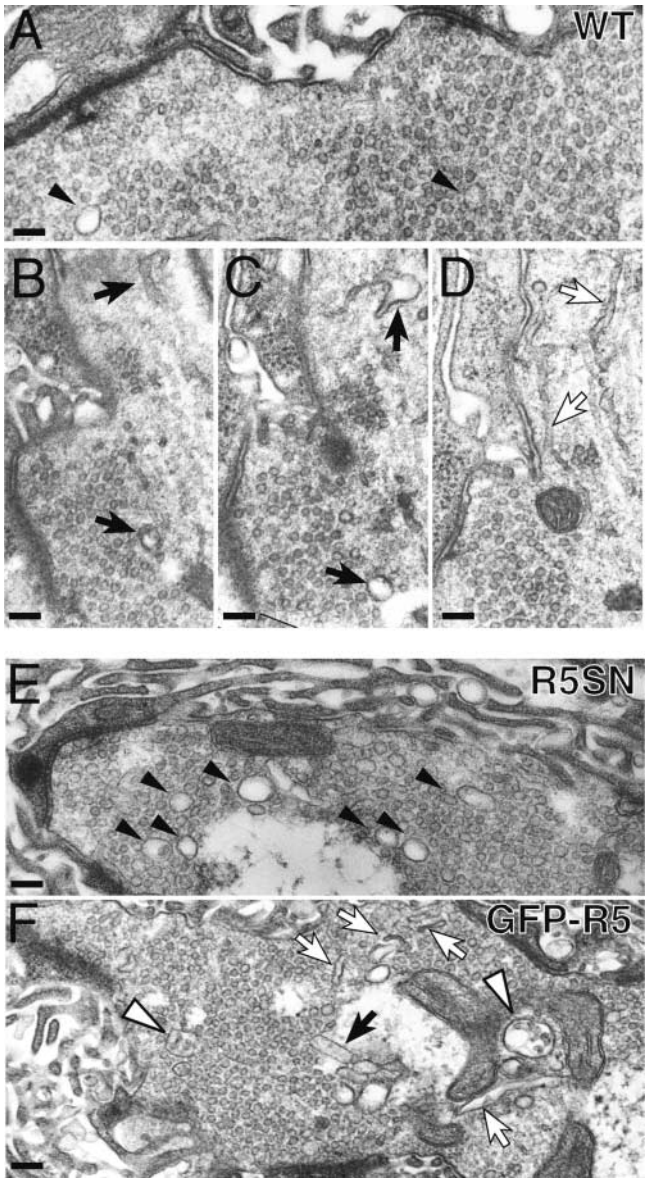


Figure 7. **Endocytic intermediates are affected in Rab5 mutant presynaptic terminals.** Ultrastructure of presynaptic terminals of wild-type (A–D), *w; UAS-Rab5S43N/+; elav-GAL4/+* (E), and *w; UAS-Rab5/+; elav-GAL4/+* third instar larvae (F). (A and E) Solid arrowheads indicate endocytic intermediates with an average diameter of 70 nm. (B–D) Electron micrographs corresponding to serial sections from a wild-type synapse showing cisternal (black arrows) and tubular (white arrows) endosomal structures. Bars, 100 nm. Cisternal structures are frequently detected in serial sections spanning 500 nm–1 μm, but are not present in each of the sections through the synapse. In Rab5S43N-expressing terminals (E), an accumulation of the 70-nm vesicles was observed (solid arrowhead). In Rab5-overexpressing terminals (F), tubules (white arrows), cisternae (black arrow), and multivesicular bodies (white arrowheads) were found in each section throughout the synapse, indicating an expansion of the endosomal compartment. No major change was observed in other synaptic features neither in Rab5S43N nor in Rab5 overexpressing terminals including the number and structure of the T-bars, the number of docked vesicles defined as vesicles touching the plasma membrane at the T-bar (WT: 1.31 ± 0.24, $n$ = 17; *Rab5S43N*: 1.67 ± 0.20, $n$ = 30; *Rab5*: 1.29 ± 0.22, $n$ = 14; *GFP-Rab*: 1.22 ± 0.18, $n$ = 10), the overall appearance of the presynaptic terminal and the subsynaptic reticulum postsynaptically.

Published May 12, 2003



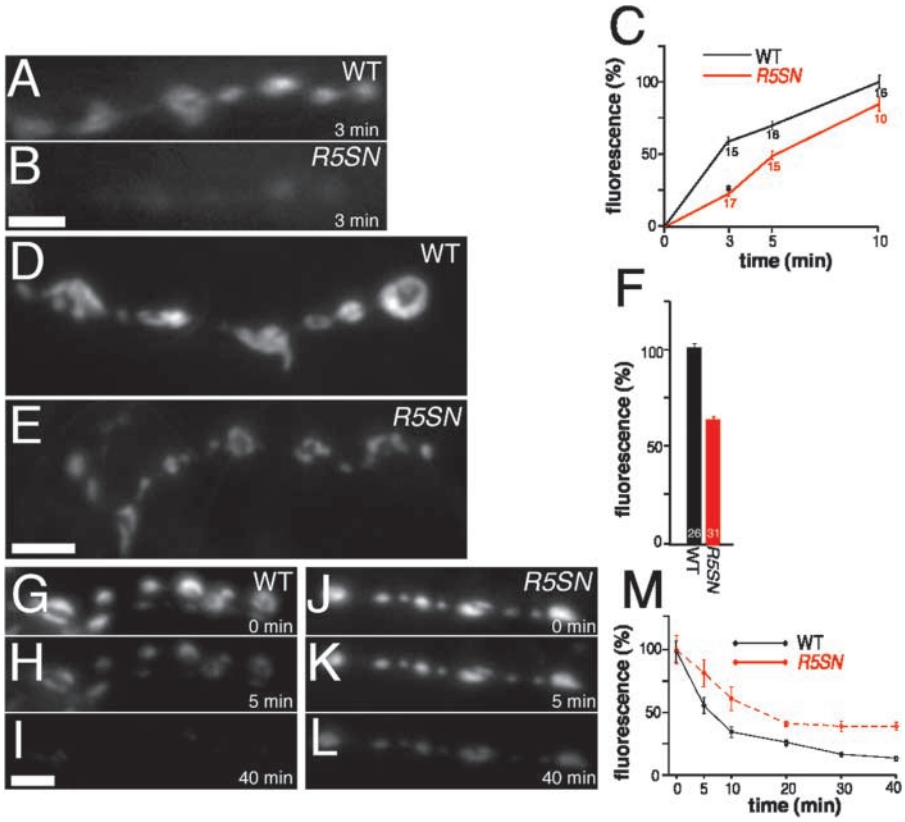


Figure 8. **Rab5 mutations affect the SV pool size and the kinetics of uptake and release.** (A–C) FM1–43 uptake. FM1–43 staining upon dye internalization for 3 min at 3 Hz (HL3, 1.5 mM $Ca^{2+}$) in (A) wild-type and (B) *w; UAS-Rab5S43N/+; elav-GAL4/+* mutant presynaptic terminals. (C) Time course of FM1–43 uptake during simulation at 3 Hz (HL3, 1.5 mM $Ca^{2+}$) for 3, 5, and 10 min in wild type (black) and *w; UAS-Rab5S43N/+; elav-GAL4/+* (red). Fluorescence refers to average pixel brightness values at the terminal normalized as percentage with respect to the average fluorescence in wild type after 10 min. In the case of *Rab5S43N*, for the uptake quantification after 3 min (asterisk), the terminals were counterstained with the red FM5–95 dye in order to be able to distinguish the terminals and quantify the low levels of uptake. Numbers in each time point correspond to the number of NMJs quantified. (D–F) Recycling SV pool size. FM1–43 staining in (D) wild-type and (E) *w; UAS-Rab5S43N/+; elav-GAL4/+* terminals after 3 min at 30 Hz (normal saline, 2 mM $Ca^{2+}$. (F) Quantification of FM1–43 internalization upon dye uptake as in D and E in wild-type (black) and *UAS-Rab5S43N/+; elav-GAL4/+* mutant terminals (red). Fluorescence is normalized as percentage with respect to the average fluorescence in wild type. Numbers in the columns are the number of NMJs analyzed. The amount of internalized FM1–43 reaches equilibrium after 3 min. Note the highly significant reduction to 64.15 ± 2.9% ($P < 0.001$; ANOVA) in the mutant. (G–M) FM1–43 release. FM1–43 fully loaded SV pool stained as in D–F in (G) wild-type and (J) *w; UAS-Rab5S43N/+; elav-GAL4/+* mutant terminals. Staining of the same wild-type (H and I) and mutant (K and L) NMJs after 5 (H and K) and 40 min (I and L) of release by stimulation at 3 Hz (normal saline, 2 mM $Ca^{2+}$). Brightness in G and J was adjusted for the best contrast of the signal and the imaging conditions were maintained in H and I and K and L, respectively. (M) Time course of FM1–43 release in wild-type (black; $n = 6$ NMJs), and *w; UAS-Rab5S43N/+; elav-GAL4/+* (red; $n = 7$ NMJs) presynaptic terminals. Terminals were first fully loaded as in D–F and fluorescence was quantified. Afterwards, they were stimulated at 3 Hz (normal saline, 2 mM $Ca^{2+}$) during 5, 10, 20, 30, and 40 min to study the release kinetics (see Materials and methods). Fluorescence refers to average brightness pixel values at the terminals normalized as percentage with respect to the average fluorescence of the fully loaded SV pool before release. Bars, 5 μm. Only presynaptic terminals of abdominal A2–A4 muscles 6/7 NMJs were analyzed.

(Fig. 8, D–F) and no further increase in the internalized fluorescence could be detected after 5 min of stimulation (unpublished data). Therefore, FM1–43 labeling under these conditions serves as an estimate of the relative SV recycling pool size. Fig. 8 (D–F) shows that blocking Rab5 function causes a significant decrease to 64.15 ± 2.9% ($n = 31$, $P <$ 0.001) in the SV recycling pool size.

Once loaded with FM1–43 using this protocol, we stimulated the synapse at 3 Hz for various periods of time, and measured the amount of dye released by quantifying the remaining fluorescence (Fig. 8, G–M; see Materials and methods). We were able to distinguish three phases during FM1–43 release in wild type (Fig. 8 M): (1) a fast release phase during the first 5 min; (2) a slower phase between 5 and 30 min; and (3) a third phase, after 30 min, when no more dye could be released and ~15% of FM1–43 dye remained unreleasable. In the mutant synapses, release occurred 2.5 times slower during the first 5 min (Fig. 8 M, also compare G and H with J and K), indicating that impaired Rab5 function reduces SV release.

In summary, these data indicate that the SV cycle is impaired in *Rab5S43N* mutant synapses. Because endocytosis and exocytosis are coupled at the *Drosophila* presynaptic terminal, it is difficult to determine if Rab5 is involved in endocytosis–endosomal trafficking, in exocytosis, or in both. However, in mammalian cells, Rab5 has been implicated in the formation of clathrin-coated endocytic vesicles (McLauchlan et al., 1998) and their subsequent fusion with the early endosome (Bucci et al., 1992; Stenmark et al., 1994). Therefore, we favor the scenario where Rab5 is involved in SV recycling.

### Rab5 function affects the SV fusion efficacy

We used standard electrophysiological recording techniques to show directly whether impaired Rab5 function affects spontaneous and $Ca^{2+}$-triggered exocytosis. We recorded spontaneous miniature excitatory junction potentials (mEJPs) and nerve-evoked EJPs in muscle 6 of third instar larvae (Fig. 9).

mEJP recordings from *Rab5S43N* mutant NMJs, displayed no significant differences in mean frequency, amplitude, variability, or voltage decay kinetics compared with wild-type mEJPs (Fig. 9, A and B). This result indicates that presynaptic expression of Rab5S43N does not affect the vesicular NT content, the number of fusion competent vesicles, or the postsynaptic glutamate receptor function or density.

Published May 12, 2003



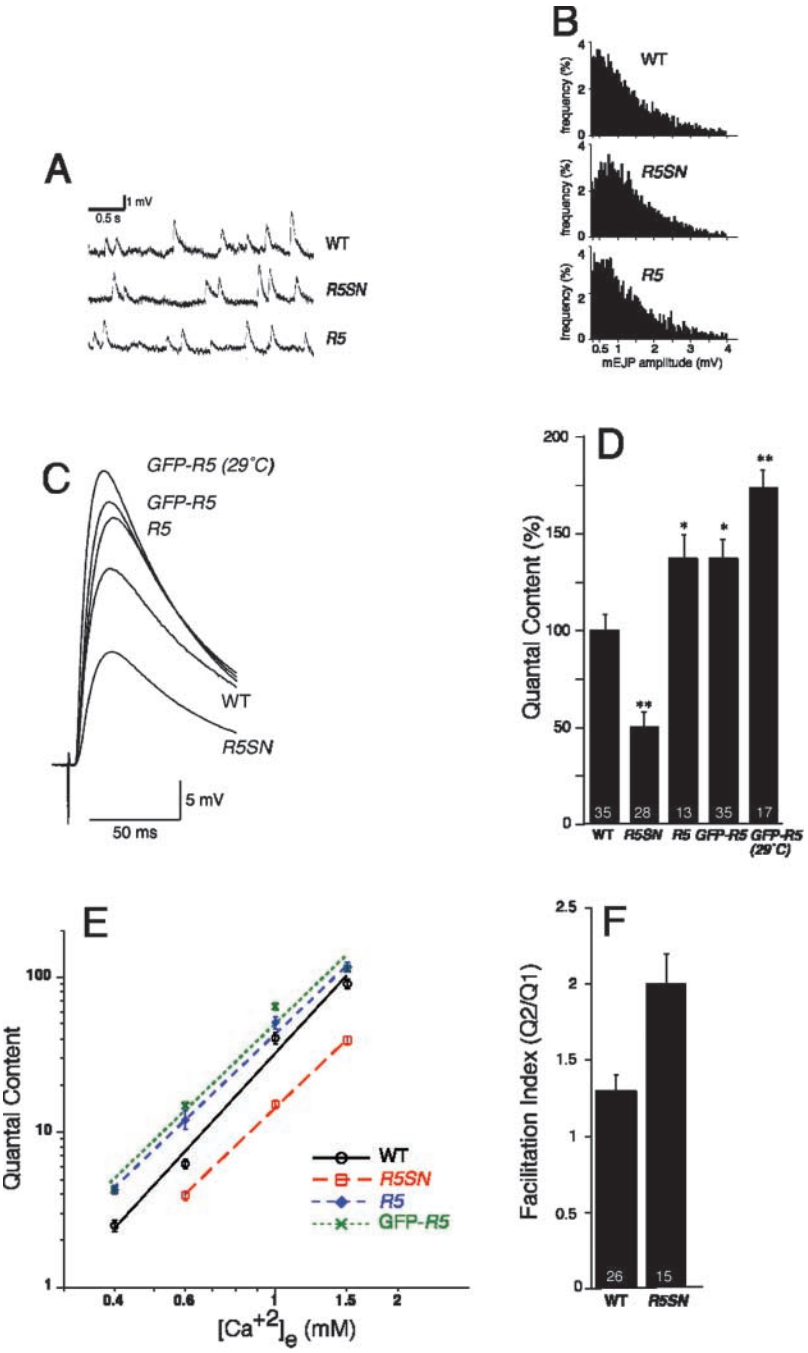


Figure 9. **NT release probability is affected in Rab5 mutant synapses.** (A) Spontaneous mEJP traces from wild-type (WT), *w; UAS-Rab5S43N/+; elav-GAL4/+* (*R5SN*), and *UAS-Rab5/+; elav-GAL4/+* (*R5*) mutant muscle 6. (B) mEJP amplitude distribution from WT, ($n$ = 6,187 events); R5SN, ($n$ = 4,395); R5, ($n$ = 3,391) NMJs. In the different genotypes studied, there were no significant differences in the mean mEJP amplitude (mV; WT, 1.3 ± 0.06, $n$ = 35; R5SN, 1.3 ± 0.06, $n$ = 28; R5, 1.3 ± 0.07, $n$ = 13 muscle 6) or mean mEJP frequency (Hz; WT, 3.7 ± 0.17, $n$ = 35; R5SN, 3.3 ± 0.23, $n$ = 28; R5, 2.8 ± 0.17, $n$ = 13 muscle 6). We also found no difference if we overexpressed the GFP-Rab5 fusion at the presynaptic terminal (mEJP amplitude [mV]: GFP-Rab5 (25°C) 1.4 ± 0.06, $n$ = 35; GFP-Rab5 (29°C), 1.2 ± 0.05, $n$ = 17. mEJP frequency (Hz): GFP-Rab5 (25°C), 3.1 ± 0.18, $n$ = 35; GFP-Rab5 (29°C), 3.0 ± 0.14, $n$ = 17). (C) Nerve-evoked EJP trace averages from wild-type and different Rab5 mutants. (Genotypes in C–F) Wild-type (WT); w; UAS-Rab5S43N/+; elav-GAL4/+ (R5SN); w; UAS-Rab5/+; elav-GAL4/+ (R5); w; elav-GAL4/UAS-GFP-Rab5 (GFP-R5); and w; elav-GAL4/UAS-GFP-Rab5 raised at 29°C during the last 2 d of larval development (GFP-R5 [29°C]). The mean amplitudes were (mV): WT; 23.5 ± 1.4; R5SN, 12.9 ± 1.2, $P < 0.01$ (ANOVA); R5, 28.0 ± 1.5, $P < 0.05$; GFP-R5, 30 ± 1.1, $P < 0.01$; GFP-Rab5 (29°C), 33 ± 1.2, $P < 0.01$. (D) Mean quantal content in wild-type and different Rab5 mutants. Quantal content is normalized as percentage of wild-type. (Numbers in columns) Number of muscle 6 analyzed. One asterisk denotes $P < 0.05$ significance values with respect to wild type, and two asterisks, $P < 0.01$. No significant difference in the evoked EJP amplitudes or quantal contents were observed in the controls submitted to the 29°C treatment when compared with animals at 25°C. (E) $Ca^{2+}$ dependence of the quantal content in WT (black ○), *R5SN* (red □), *R5* (blue ◆), and *GFP-R5* (green ×). (F) Facilitation index calculated as mean ratio of the quantal contents of the second versus the first response in a paired pulse stimulation protocol with a 20-ms interpulse interval. (Numbers in the columns) Number of muscles 6 analyzed. Q2/Q1 was significantly higher ($P < 0.05$) in *Rab5S43N* with respect to wild-type. The recording solution used in A–D and F consisted of HL3 containing 0.75 mM $Ca^{2+}$.

This is consistent with the normal synaptic ultrastructure (Fig. 7), mean number of active zones (Fig. 6 E), and mean number of docked vesicles at the T-bar (Fig. 7, statistical analysis therein) of the mutant NMJs as shown above.

Next, we addressed the efficacy of evoked synaptic transmission. EJPs were evoked by stimulating the segmental nerve, and the voltage response in the muscle was recorded (Fig. 9 C). We calculated the number of vesicles fusing upon arrival of a single action potential, the quantal content, from the mean EJP amplitude at a basal stimulation frequency of 0.5 Hz and from the mean mEJP amplitude measured in the same muscle (see Materials and methods; Martin, 1955). We observed that the mean quantal content was reduced to 49.8 ± 2.0% ($n$ = 28) in Rab5S43N-expressing terminals when compared with wild-type larvae (Fig. 9 D), consistent with a decreased FM1–43 release rate in the mutant (Fig. 8, G–M).

Furthermore, Rab5S43N-expressing synapses show a stronger paired-pulse facilitation than wild-type synapses. In wild-type synapses, responses show a slightly facilitated paired-pulse ratio (Q2/Q1) of 1.3 ± 0.1 ($n$ = 26) at a 20-ms interpulse interval using an external $Ca^{2+}$ concentration ($[Ca^{2+}]_e$) of 0.75 mM (Fig. 9 F). In contrast, Rab5S43N-expressing terminals show a significantly stronger facilitation and exhibited a Q2/Q1 ratio of 2.0 ± 0.2 ($n$ = 15, $P <$ 0.05). Because the paired-pulse ratio was increased, the number of docked vesicles (Fig. 7, statistical analysis therein) and the spontaneous release rate were normal in Rab5S43N-expressing synapses, these data indicate that impaired Rab5

Published May 12, 2003



function lead to a reduced probability of the $Ca^{2+}$-triggered release of SVs.

Because the $Ca^{2+}$-triggered release probability was reduced, we next studied the $Ca^{2+}$ sensitivity and $Ca^{2+}$ cooperativity during NT release by systematically examining the quantal content as a function of the $[Ca^{2+}]_e$ (Fig. 9 E). The slope of the $Ca^{2+}$dependency of the mean quantal content was not affected in the mutant synapses (Fig. 9 E), reflecting a normal $Ca^{2+}$cooperativity and indicating that $Ca^{2+}$ binding to the $Ca^{2+}$ sensor was not affected. However, for all $[Ca^{2+}]_e$ examined, the release probability in *Rab5S43N* was significantly reduced (Fig. 9 E) indicating that the defect induced by interfering with Rab5 function is likely to be $Ca^{2+}$ independent and probably affects the efficacy of the evoked SV fusion process itself. This can be either due to a reduced number of fusion competent vesicles or to a reduced efficacy of vesicular release. The observation that the mEJP frequency (Fig. 9, A and B) as well as the number of active zones and docked vesicles (Fig. 6, B–E, and Fig. 7 E [statistical analysis therein]) are normal in *Rab5S43N* implies that it is the probability of SV fusion that is affected in the mutant. Therefore, we conclude that Rab5-dependent endosomal trafficking affects the efficacy of $Ca^{2+}$-triggered exocytosis at the presynaptic terminal.

### Rab5-mediated trafficking is rate-limiting during endocytic trafficking and synaptic transmission

We have shown above that inhibition or Rab5 function reduces the endo- and exocytosis rates and the SV recycling pool size. To address if Rab5 function is rate-limiting, we overexpressed Rab5 in the CNS and monitored the kinetics of recycling, synaptic transmission, and the ultrastructure of the synapse. To overexpress Rab5, we took advantage of the thermosensitivity of GAL4 in *Drosophila* (Brand et al., 1996; Entchev et al., 2000) using elav-GAL4 at either 25°C or 29°C during the last two days of larval development (see Materials and methods).

Like in cultured mammalian cells (Bucci et al., 1992), Rab5 overexpression at the presynaptic terminal causes expanded endosomal structures (Fig. 7 F). Thus, in each random EM section through the Rab5 overexpressing terminals, we observed large tubular structures (Fig. 7 F, white arrows) and multivesicular bodies (Fig. 7 F, white arrowheads), unlike in wild-type synapses where cisternal structures were only occasionally found in any given random section. This is consistent with our finding that only one to three endosomal structures are present per synaptic bouton (Fig. 2, A, E, and F). Furthermore, FM1–43 internalization rates were significantly increased up to 118 ± 4.4% ($n$ = 14; $P < 0.05$; 3 Hz 10 min) at 1.5 mM $[Ca^{2+}]_e$ and up to 158.82 ± 4.5% ($n$ = 16, $P < 0.0001$; 3 Hz 15 min) at 0.75 mM $[Ca^{2+}]_e$ in Rab5 overexpressing terminals with respect to controls (unpublished data). Therefore, similar to mammalian cells (Bucci et al., 1992), Rab5 overexpression causes an increase in the endocytic rate, as reflected by the internalization rate and expanded endosomal structures.

To address the effect of Rab5 overexpression on the efficacy of vesicular release, we recorded mEJPs and EJPs and calculated the quantal content upon basal stimulation at 0.5 Hz. mEJPs of Rab5 overexpressing synapses displayed no significant differences in the mean amplitude, variability, frequency, or voltage decay kinetics compared with wild type (Fig. 9, A and B). This indicates that the vesicular NT content, the number of fusion competent SVs, and the postsynaptic glutamate receptor function and density are normal in the overexpressing terminals. Consistently, a normal number of docked vesicles was observed at the ultrastructural level (Fig. 7 F, statistical analysis therein) and no difference in the overall morphology, synaptic surface area, or active zones could be detected (Fig. 6, A, D, and E; unpublished data).

The mean quantal content, however, was significantly increased, up to 1.74-fold of wild type (Fig. 9 D). Because the number of docked vesicles and the spontaneous release rate were normal, the higher quantal content indicates that elevated levels of Rab5 function led to an increased probability of the $Ca^{2+}$-triggered SV release. The slope of the $Ca^{2+}$ dependency of the quantal content was not affected (Fig. 9 E). We conclude that Rab5 functions in a rate-limiting manner in a $Ca^{2+}$-independent step during the SV fusion process.

## Discussion

Here, we have described the presence of a Rab5-positive, PI(3)P-containing endosomal compartment at the presynaptic terminal of *Drosophila*. As in nonneuronal cells, this compartment depends on Rab5 function. We have shown that the endosome is depleted under conditions where SVs are depleted and that the endosome is replenished by membrane derived by dynamin-mediated endocytosis. Rab5 also influences the synaptic efficacy: impairment of Rab5 function decreases the NT release probability and the recycling SV pool size, whereas overexpression of Rab5 increases the release probability. Our working model is that membrane exchange between the vesicle pool and the presynaptic endosome occurs and is of functional importance for the efficiency of SVs to fuse with the plasma membrane during $Ca^{2+}$-triggered endocytosis.

### Membrane exchange between the vesicles pool and the synaptic endosome

The mechanism of SV recycling has since long been a matter of debate (Jarousse and Kelly, 2001; Valtorta et al., 2001). It has been proposed that vesicles internalized by clathrin-mediated endocytosis traffic through an intermediate endosomal compartment to become mature SVs (Hannah et al., 1999; Jarousse and Kelly, 2001). However, in cultured hippocampal neurons, endocytic vesicle membrane does not intermix with an internal intermediate compartment (Murthy and Stevens, 1998; Zenisek et al., 2000). Our results present evidence that Rab5-dependent membrane exchange between vesicles and the endosome at the synapse can occur. Furthermore, we showed that a Rab5-mediated trafficking step determines, in a rate-limiting manner, the synaptic performance.

It has been previously established that Rab5 is involved in the fusion of endocytic vesicles with their target endosomal compartment (Bucci et al., 1992; Stenmark et al., 1994). In addition Rab5 has been implicated in the budding of endocytic vesicles from the plasma membrane (McLauchlan et al., 1998). Our data are consistent with a key role of Rab5 during both endocytic trafficking steps at the presynaptic

Published May 12, 2003



terminal. This is because exocytosis and endocytosis are temporally and functionally coupled at the *Drosophila* NMJ, making it difficult to ascertain the primary basis of an endo- or exocytic/recycling phenotype. Because the ultrastructure of the endosome is grossly disrupted in Rab5 loss- and gain-of-function mutants (Fig. 7), we favor, however, the possibility that it is the Rab5-dependent endosomal dynamics that play a key role in the SV cycle.

Our data leaves open the question whether this proposed trafficking step is obligatory during SV recycling or if it involves trafficking of only an SV sub-pool at any given time. However, regardless of what percentage of the SV pool recycles at a given time through the endosome, at the steady state, this recycling pathway must play a key role for the synaptic performance of the full SV pool, because synaptic efficacy increases or decreases in a rate-limiting manner depending on the levels of Rab5 function.

### What could be the function of the endosome at the presynaptic terminal?

Interfering with Rab5 function using the dominant-negative version of Rab5 causes a reduction in the number of released quanta during synaptic transmission, whereas elevated levels of Rab5 increase the quantal content. Our morphological and electrophysiological analysis of these Rab5 mutants shows that the changes in synaptic performance are not due to a change in the readily releasable pool size (Neher and Zucker, 1993; Kuromi and Kidokoro, 1998; Delgado et al., 2000), but are rather due to a change in the release probability of the SVs.

How could the membrane exchange between vesicles and the endosome affect the SV release probability? It is well established in cultured mammalian cells that the Rab5 endosome functions as a sorting station where endocytic cargo is targeted either toward recycling or degradation (Zerial and McBride, 2001). We speculate that a similar scenario may take place within the presynaptic terminal. The protein and lipid composition of the SV membrane could be controlled at the endosome by sorting out aged components and replacing them with newly synthesized ones. This, in turn, will be likely of consequence for SV function, particularly for the efficacy of regulated exocytosis and, therefore, for the SV release probability. Furthermore, sorting of alternative vesicular proteins could occur at the endosome. In this context, it has been recently found that the ratio of different Synaptotagmin isoform (Synaptotagmin I vs. Synaptotagmin IV) in SVs affects the efficacy of $Ca^{2+}$-triggered exocytosis (Chapman et al., 1998; Osborne et al., 1999).

Based on our findings that enhancement or reduction of Rab5 function lead to a parallel increase or decrease in the SV release probability, we suggest that a Rab5-mediated membrane exchange between vesicles and the endosome affects the synaptic strength in a rate-limiting manner.

## Materials and methods

### Molecular analysis and mutant strains

The exon–intron organization of Rab5 (GenBank/EMBL/DDBJ accession no. BK000968) was based on 11 cDNAs, as well as genomic sequence information from the Berkeley *Drosophila* Genome Project (BDGP). We sequenced two cDNAs, GM02432 and LD03788 (GenBank/EMBL/DDBJ accession nos. AY081180, AY081181), and used 5′ and 3′ sequence information from BDGP for nine other cDNAs (LD39028, GH28628, GH22603, LD05288, LD22469, GH26712, GH21777, GH15713, and GH28615). Alternative splicing generates two major Rab5 mRNA size classes of around 1 and 1.8 kb, consistent with two bands in Northern blot experiments using the ORF as a probe (unpublished data). The genes flanking Rab5 are a zinc-finger transcription factor (CG4272) and a Heparansulphate proteoglycan (CG7245; Fig. 5 A). One of the Rab5 splicing forms overlaps by 28 bp with the 5′ end of the CG4272 transcript (Fig. 5 A).

*shibire$^{ts}$*, *elav-GAL4* (flybase), *UAS-DRab5*, and *UAS-DRab5S43N* have been described previously (Entchev et al., 2000). Oregon-R was used as the wild-type strain. In UAS-GFP-Rab5, EGFP (CLONTECH Laboratories, Inc.) was cloned $NH_2$ terminally to the ORF of DRab5. In the chimera, GFP remains attached to Rab5 as shown by colocalization of anti-DRab5 and anti-GFP antibodies in NMJs expressing GFP-Rab5. *UAS-GFP-Rab5S43N* was generated by in vitro mutagenesis. The *myc-2xFYVE* sequence was PCR cloned from pGEM–myc-2xFYVEHrs (Gillooly et al., 2000) into pUAST. *GFP–myc-2xFYVE* is an $NH_2$-terminal EGFP fusion to the same myc-2xFYVE chimera. Transgene expression in the nervous system was driven by elav-GAL4 and represented around fivefold the levels of endogenous Rab5 as estimated in Western blots using larval CNS extracts. The *P(w$^+$)DRab5$^+$* rescue construct was generated by PCR cloning of a genomic fragment amplified from a wild-type fly extract using primers from the 5′ and 3′ ends of the CG4272 and CG7245 flanking genes into the pCaSpeR4 vector, respectively.

*Rab5$^1$* is a P-element lethal insertion from the Kiss collection, *P{lacw}Rab5K08232*. If raised under "intensive care" conditions (Loewen et al., 2001), very few *Rab5$^1$* larvae developed into adult flies, which display a flightless phenotype. *Rab5$^1$* homozygous adults are poorly fertile. *Rab5$^1$* phenotype and lethality were reverted by precise excision of the P-element. *Rab5$^1$* was rescued by P(w$^+$)DRab5$^+$ or expression of GFP-Rab5 in the nervous system using elav-GAL4. *Rab5$^2$*, *Rab5$^3$*, and *Rab5$^4$* were generated by imprecise excision of the P-element and their lesions determined by PCR cloning and sequencing of the Rab5 gene in the different mutants. *Rab5$^2$* is a 4-kb deletion of Rab5. Although *Rab5$^2$* also deletes parts of the 5′-nontranslated leader of CG4272, the lethality and phenotype of *Rab5$^2$* are caused by loss of Rab5 function because both are rescued by P(w$^+$)DRab5$^+$, a rescue construct spanning Rab5 and excluding the two flanking genes (Fig. 5 A). *Rab5$^3$* is an 18 + 210-bp insertion of sequences from the left and right long terminal repeat (LTR) of the P-element, which remained after imprecise excision of the transposon. *Rab5$^4$* is a 14-bp insertion of the right LTR of the P-element. *Rab5$^3$* and *Rab5$^4$* are homozygous viable and show a flightless phenotype in 88 and 63% of adult flies, respectively. Both mutants show a decrease in the Rab5 protein levels (46 and 36% of wild-type levels, respectively) as determined in Western blot experiments using the anti-DRab5 antibodies.

### Antibodies and immunohistochemistry

Rabbit anti–*Drosophila* Rab5 antibody was generated by Eurogentec against a COOH-terminal peptide (H2N-TSIRPTGTETNRPTNN-CONH2). The immune serum was affinity chromatography purified using the Rab5 peptide coupled to CNBr-activated Sepharose 4B (Amersham Biosciences). The antibody detected a single band of the expected size (24 kD) in Western blots. Antibody-specificity was tested by preincubating the purified antibody with 100 μg/ml Rab5 peptide for 30 min at RT followed by an antibody staining on GFP-Rab5 overexpressing NMJs where no signal was detected. Preincubation with a control peptide did not affect the staining. For Western blot experiments the blot was incubated with anti-Rab5 (1:200), anti-GFP (1:200; Santa Cruz Biotechnology, Inc.), anti-tubulin (1:400; DSHB), or anti-actin antibody (1:200; Sigma-Aldrich). Quantification was done using the Image Gauge software (Fuji).

Immunofluorescence of third instar NMJs or embryos was performed as described (González-Gaitán and Jäckle, 1997) with minor modifications. Antibodies were diluted in PEM (80 mM Pipes, 5 mM EGTA, 1 mM $MgCl_2$, pH 7.4) containing 0.1% IGEPAL (Sigma-Aldrich) and used in the following concentrations: rabbit anti–α-adaptin 1:50 (González-Gaitán and Jäckle, 1997), mouse anti-CSP 1:100 (Zinsmaier et al., 1990), mouse anti-Fasciclin II (1D4) 1:20 (Schuster et al., 1996a), mouse anti-nc82 1:100 (Heimbeck et al., 1999), rabbit anti-HRP 1:50 (Sigma-Aldrich), mouse anti–c-myc 1:50 (Calbiochem), rabbit anti-DRab5 1:50. Secondary Alexa 546– or Alexa 488–conjugated antibodies (Molecular Probes) were used (1:500). Quantification of the synaptic area of NMJs from muscles 6/7 in segment A2 was performed on projections of z-sections acquired after anti-CSP staining. The synaptic area was determined by thresholding the images using the MetaView software (Visitron Systems). The percentage of

Published May 12, 2003



synaptic surface was calculated with respect to the combined rectangular surface area of muscles 6 and 7. To quantify the number of active regions per presynaptic terminal, preparations were stained with mouse anti-nc82 to label active zones and rabbit anti–α-adaptin or anti-dynamin to label the centers of endocytosis. Active zones labeled by the nc82 staining were counted and normalized to the area of the presynaptic terminal.

### EM and immuno-EM

For EM, third instar larvae were dissected in normal saline and processed as described (Wu et al., 1998) with minor modifications. For immuno-EM flat preparations of third instar larvae were fixed in 4% PFA and 0.05 or 0.2% glutaraldehyde (GA), embedded in 10% gelatine, and infiltrated in 2.3 M sucrose. Specimens were quickly frozen in liquid nitrogen and cryosectioned with a Leica ultracut UCT/FCS equipment (Leica) at −105°C and 80-nm cryosections retrieved in 1% methylcellulose (Sigma-Aldrich)/1.3 M sucrose (Merck). Cryosections were incubated with anti-GFP, anti-CSP, and/or anti-Rab5 antibodies, and a 10- or 5-nm gold-coupled secondary antibody. Subsequently, sections were incubated in 1% GA and 0.3% uranylacetate/1.8% methylcellulose, and imaged with a Morgagni electron microscope (FEI Co.).

### Salines

Normal saline (Jan and Jan, 1976) had the following composition (mM): 130 NaCl, 5 KCl, 5 Hepes, 2 $MgCl_2$, 2 $CaCl_2$, 36 sucrose, pH 7.3. High $K^+$ was composed of (mM): 80 NaCl, 60 KCl, 5 Hepes, 2 $MgCl_2$, 2 $CaCl_2$, 36 sucrose, pH 7.3. HL3 (Stewart et al., 1994) consisted of (mM): 70 NaCl, 5 KCl, 20 $MgCl_2$, 10 $NaHCO_3$, 5 Trehalose, 115 sucrose, 5 Hepes, 0.75 or 1.5 $CaCl_2$, pH 7.2. For $Ca^{2+}$-free normal saline or $HL_3$ $CaCl_2$ was exchanged against $MgCl_2$.

### Electrophysiology

Current clamp recordings were performed as described previously (Schuster et al., 1996b) with minor modifications. In brief, EJPs of muscle 6 in segments A2–A4 were evoked with a stimulation–isolation unit A360 (World Precision Instruments, Inc.). Only recordings with resting membrane potentials of at least −60 mV and input resistances of at least 6 MΩ were used. Voltage signals were amplified with a SEC-0.5L amplifier (npi), filtered at 2 kHz, digitized using a DIGIDATA 1320A (Axon Instruments, Inc.), recorded and analyzed with Axograph Software (Axon Instruments, Inc.). The mean EJP amplitude was determined by averaging 30 single EJPs evoked at 0.5 Hz. The quantal content was calculated by dividing the mean EJP amplitude of a certain muscle by the mean mEJP recorded in the same muscle and was corrected for nonlinear summation according to Martin (1955) using a reversal potential as described (Nishikawa and Kidokoro, 1995). mEJPs were recorded for 1 min after the EJPs at 0.5 Hz and were analyzed using the event detection feature of Axograph. For comparison of the mEJPs between different mutants, mEJPs recorded in HL3 containing 0.75 mM $Ca^{2+}$ were used. The groups were closely matched concerning their mean resting potentials (66 to 71 mV) and mean input resistances (7.0 to 8.5 MΩ). Paired-pulse facilitation experiments were performed in $HL_3$ containing 0.75 mM $Ca^{2+}$ by delivering two stimuli with an interpulse interval of 20 ms with a 5-s rest and averaging 20 paired stimuli. The degree of facilitation was calculated by dividing the quantal content of the second by the quantal content of the first response. $Ca^{2+}$ dependency was determined in a separate set of experiments using EJPs recorded in $HL_3$ containing 0.4, 0.6, 1.0, and 1.5 mM $Ca^{2+}$ at 0.5 Hz. More than 10 NMJs were analyzed for each $Ca^{2+}$ condition. In control experiments, no significant statistical difference (ANOVA) in the EJP amplitude was observed between WT synapses and the elav-GAL4 control siblings (genotype: w; elav-GAL4/TM3-GFP or w; Cyo-GFP/+; elav-GAL4/+) of the Rab5S43N or Rab5 overexpressing synapses.

### Dye imaging

Wandering third instar larvae were dissected in ice-cold, $Ca^{2+}$-free normal saline or $HL_3$, the brain and ventral cord were removed, and the preparation was rinsed with the same saline used for dye-uptake. Dye-uptake was induced by stimulating the segmental nerves at 3 or 30 Hz in the presence of 10 μM FM1–43 (Molecular Probes) in either normal saline or $HL_3$ containing 0.75 or 1.5 mM $Ca^{2+}$. Washing was done in either $Ca^{2+}$-free normal saline or $Ca^{2+}$-free $HL_3$ in the dark, rinsing first thoroughly and then superperfusing for 20 or 30 min. The recycling pool of SVs was fully labeled after stimulation for 3 min at 30 Hz because an increase in the stimulation time did not increase the fluorescence within the terminals. Release experiments were performed at 3 Hz in normal saline after imaging a single fully loaded NMJ. Stimulation was interrupted after 5, 10, 20, 30, and 40 min and the NMJ was imaged again. Images were acquired with a CCD camera (Diagnostic Instruments), controlled by MetaView imaging software. The illumination of the field and the absolute fluorescence intensity were checked by imaging a homogeneously fluorescent calibration slide (Applied Precision). For quantitative measurements, only presynaptic terminals of the NMJ of muscles 6/7 that were clearly in focus were used, measuring the average intensity of each terminal using MetaView and substracting background fluorescence of the muscle near the terminal.

For the FM5–95 uptake experiments,15 μM FM5–95 (Molecular Probes) was used either in high $K^+$ solution for 1 min or in normal saline stimulating segmental nerves 3 min at 30 Hz. The preparation was washed for 30 min in $Ca^{2+}$-free saline before imaging. In a set of control experiments we checked that FM5–95 was not internalized in $shi^{ts1}$ at the restrictive temperature or in the absence of stimulation (unpublished data). In control experiments, no significant statistical difference (ANOVA) in the FM1–43 uptake rate or the steady-state loading was observed between WT synapses and the elav-GAL4 control siblings (genotype: w; elav-GAL4/TM3-GFP or w; Cyo-GFP/+; elav-GAL4/+) of the Rab5S43N or Rab5 overexpressing synapses. Dextran uptake in cultured *Drosophila* S2 cells was performed by incubating the cells for 5 min at RT with 0.5 mM Texas red–dextran (3,000 MW, lysine fixable; Molecular Probes) in complete Schneider medium. Subsequent washing steps were performed on ice, followed by the fixation in 4% PFA in PEM for 60 min.

### $shi^{ts}$ depletion–recovery and wortmannin experiments

For the $shi^{ts}$ depletion–recovery experiments, $shi^{ts}$ third instar NMJs expressing GFP-2xFYVE in the CNS were imaged in normal saline in resting conditions or after stimulation at 3 Hz for 30 min or 30 Hz for 10 min. Depletion of the endosome was performed by stimulating the synapse at the restrictive temperature (around 33°C) at 3 or 30 Hz for different time intervals. Recovery was performed in normal saline at RT. For the quantification fluorescence measured near the endosomes was subtracted.

For the wortmannin treatment, GFP-Rab5 or GFP-2xFYVE expressing NMJs were imaged in vivo using a confocal microscope (LSM 510; Carl Zeiss MicroImaging, Inc.). The preparations were then incubated in 100 nM wortmannin (Sigma-Aldrich) in $Ca^{2+}$-free saline for 45 min at RT. After fixation for 90–120 min in 4% PFA in PEM the same NMJs were imaged again. No change was seen in the control containing DMSO without wortmannin. The GFP-Rab5 pattern was not affected even if wortmannin was used at 250 nM for 45 min as previously reported for mammalian cells (Sonnichsen et al., 2000).

We thank A. Schwabedissen for her excellent technical assistance. We also thank R. Fernández de la Fuente and H. Taubert for the Northern data and the generation of various transgenic lines; C. Rosenmund who introduced us to the electrophysiology; H. Jäckle for supporting us in his department; S. Albert for early advice in the Rab project; A. Prokop, D. Bakasch, D. Kötting, D. Herzog, G. Dowe, G. Wiebe, and K. Anderson for their various contributions; E. Buchner, S. Sigrist, G. Tear, U. Thomas, and C. Goodman for sending us various reagents; H. Stenmark for sharing with us the myc-2xFYVE before publication; and H. Bellen, T. Kurzchalia, M. Zerial, W. Huttner, B. Betz, K. Broadie, and E. Tanaka for comments to the manuscript.

This work was supported by the Max-Planck Society and Deutsche Forschungsgemeinschaft.

Submitted: 19 November 2002
Revised: 19 March 2003
Accepted: 19 March 2003

## References

Atwood, H.L., C.K. Govind, and C.F. Wu. 1993. Differential ultrastructure of synaptic terminals on ventral longitudinal abdominal muscles in *Drosophila* larvae. *J. Neurobiol.* 24:1008–1024.

Betz, W.J., and G.S. Bewick. 1992. Optical analysis of synaptic vesicle recycling at the frog neuromuscular junction. *Science.* 255:200–203.

Betz, W.J., and G.S. Bewick. 1993. Optical monitoring of transmitter release and synaptic vesicle recycling at the frog neuromuscular junction. *J. Physiol.* 460: 287–309.

Blumstein, J., V. Faundez, F. Nakatsu, T. Saito, H. Ohno, and R.B. Kelly. 2001. The neuronal form of adaptor protein-3 is required for synaptic vesicle formation from endosomes. *J. Neurosci.* 21:8034–8042.

Brand, A., A.S. Manoukian, and N. Perrimon. 1996. Ectopic expression in *Dro-*

*sophila*. *In Drosophila melanogaster*: Practical Uses in Cell and Molecular Biology. L.S.B. Goldstein and E.A. Fyrberg, editors. Academic Press, San Diego. 635–654.

Brand, A.H., and N. Perrimon. 1993. Targeted gene expression as a means of altering cell fates and generating dominant phenotypes. *Development.* 118:401–415.

Bucci, C., R.G. Parton, I.H. Mather, H. Stunnenberg, K. Simons, B. Hoflack, and M. Zerial. 1992. The small GTPase Rab5 functions as a regulator factor in the early endocytic pathway. *Cell.* 70:715–728.

Ceccarelli, B., W.P. Hurlbut, and A. Mauro. 1973. Turnover of transmitter and synaptic vesicles at the frog neuromuscular junction. *J. Cell Biol.* 57:499–524.

Chapman, E.R., R.C. Desai, A.F. Davis, and C.K. Tornehl. 1998. Delineation of the oligomerization, AP-2 binding, and synprint binding region of the C2B domain of synaptotagmin. *J. Biol. Chem.* 273:32966–32972.

Chavrier, P., R.G. Parton, H.P. Hauri, K. Simons, and M. Zerial. 1990. Localization of low molecular weight GTP binding proteins to exocytic and endocytic compartments. *Cell.* 62:317–329.

Christoforidis, S., M. Miaczynska, K. Ashman, M. Wilm, L.Y. Zhao, S.C. Yip, M.D. Waterfield, J.M. Backer, and M. Zerial. 1999. Phosphatidylinositol-3-OH kinases are Rab5 effectors. *Nat. Cell Biol.* 1:249–252.

de Hoop, M.J., L.A. Huber, H. Stenmark, E. Williamson, R.G. Parton, and C. Dotti. 1994. The involvement of the small GTP-binding protein Rab5a in neuronal endocytosis. *Neuron.* 13:11–22.

De Renzis, S., B. Sonnichsen, and M. Zerial. 2002. Divalent Rab effectors regulate the sub-compartmental organization and sorting of early endosomes. *Nat. Cell Biol.* 4:124–133.

de Wit, H., Y. Lichtenstein, H.Y. Geuze, R.B. Kelly, P. van der Sluijs, and J. Klumperman. 1999. Synaptic vesicles form by budding from tubular extensions of sorting endosomes in PC12 cells. *Mol. Biol. Cell.* 10:4163–4176.

Delgado, R., C. Maureira, C. Oliva, Y. Kidokoro, and P. Labarca. 2000. Size of vesicle pools, rates of mobilization, and recycling at neuromuscular synapses of a *Drosophila* mutant, shibire. *Neuron.* 28:941–953.

Entchev, E.V., A. Schwabedissen, and M.A. González-Gaitán. 2000. Gradient formation of the TGF-beta homolog Dpp. *Cell.* 103:981–991.

Estes, P.S., J. Roos, A. van der Bliek, R.B. Kelly, K.S. Krishnan, and M. Ramaswami. 1996. Traffic of Dynamin within individual *Drosophila* synaptic boutons relative to compartment-specific markers. *J. Neurosci.* 16:5443–5456.

Faundez, V., J.T. Horng, and R.B. Kelly. 1998. A function for the AP3 coat complex in synaptic vesicle formation from endosomes. *Cell.* 93:423–432.

Fergestad, T., S. Davis Warren, and K. Broadie. 1999. The stoned proteins regulate synaptic vesicle recycling in the presynaptic terminal. *J. Neurosci.* 19: 5847–5860.

Fesce, R., F. Grohovaz, F. Valtorta, and J. Meldolesi. 1994. Neurotransmitter release: fusion or "kiss-and-run"? *Trends Cell Biol.* 4:1–4.

Fialka, I., P. Steinlein, H. Ahorn, G. Bock, P.D. Burbelo, M. Haberfellner, F. Lottspeich, K. Paiha, C. Pasquali, and L.A. Huber. 1999. Identification of syntenin as a protein of the apical early endocytic compartment in Madin-Darby canine kidney cells. *J. Biol. Chem.* 274:26233–26239.

Fischer von Mollard, G., B. Stahl, C. Walch-Solimena, K. Takei, L. Daniels, A. Kohklatchev, P. De Camilli, T.C. Sudhof, and R. Jahn. 1994. Localization of Rab5 to synaptic vesicles identifies endosomal intermediates in synaptic vesicle recycling pathway. *Eur. J. Cell Biol.* 65:319–326.

Gillooly, D.J., I.C. Morrow, M. Lindsay, R. Gould, N.J. Bryant, J.M. Gaullier, R.G. Parton, and H. Stenmark. 2000. Localization of phosphatidylinositol 3-phosphate in yeast and mammalian cells. *EMBO J.* 19:4577–4588.

González-Gaitán, M.A., and H. Jäckle. 1997. Role of *Drosophila* α-adaptin during synaptic vesicle recycling. *Cell.* 88:767–776.

Grant, B., and D. Hirsh. 1999. Receptor-mediated endocytosis in the *Caenorhabditis elegans* oocyte. *Mol. Biol. Cell.* 10:4311–4326.

Hannah, M.J., A.A. Schmidt, and W.B. Huttner. 1999. Synaptic vesicle biogenesis. *Annu. Rev. Cell Dev. Biol.* 15:733–798.

Heimbeck, G., V. Bugnon, N. Gendre, C. Haberlin, and R.F. Stocker. 1999. Smell and taste perception in *Drosophila melanogaster* larva: toxin expression studies in chemosensory neurons. *J. Neurosci.* 19:6599–6609.

Helenius, A., I. Mellman, D. Wall, and A. Hubbard. 1983. Endosomes. *Trends Biochem. Sci.* 8:245–250.

Heuser, J.E., and T.E. Reese. 1973. Evidence for recycling of synaptic vesicle membrane during transmitter release at the frog neuromuscular junction. *J. Cell Biol.* 57:315–344.

Hinshaw, J.E., and S.L. Schmid. 1995. Dynamin self-assembles into rings suggesting a mechanism for coated vesicle budding. *Nature.* 374:190–192.

Horiuchi, H., R. Lippe, H.M. McBride, M. Rubino, P. Woodman, H. Stenmark, V. Rybin, M. Wilm, K. Ashman, M. Mann, and M. Zerial. 1997. A novel rab5 gdp/gtp exchange factor complexed to rabaptin-5 links nucleotide exchange to effector recruitment and function. *Cell.* 90:1149–1159.

Jan, L.Y., and J.N. Jan. 1976. Properties of the larval neuromuscular junction in *Drosophila melanogaster*. *J. Physiol.* 262:189–214.

Jarousse, N., and R.B. Kelly. 2001. Endocytotic mechanisms in synapses. *Curr. Opin. Cell Biol.* 13:461–469.

Jia, X.X., M. Gorczyca, and V. Budnik. 1993. Ultrastructure of neuromuscular junctions in *Drosophila*: comparison of wild type and mutants with increased excitability. *J. Neurobiol.* 24:1025–1044.

Koenig, J.H., and K. Ikeda. 1996. Synaptic vesicles have two distinct recycling pathways. *J. Cell Biol.* 135:797–808.

Koenig, J.H., and K. Ikeda. 1989. Disappearance and reformation of synaptic vesicle membrane upon transmitter release observed under reversible blockage of membrane retrieval. *J. Neurosci.* 9:3844–3860.

Koenig, J.H., and K. Ikeda. 1999. Contribution of active zone subpopulation of vesicles to evoked and spontaneous release. *J. Neurophysiol.* 81:1495–1505.

Koenig, J.H., K. Yamaoka, and K. Ikeda. 1993. Calcium-induced translocation of synaptic vesicles to the active site. *J. Neurosci.* 13:2313–2322.

Kosaka, T., and K. Ikeda. 1983. Possible temperature-dependent blockage of synaptic vesicle recycling induced by a single gene mutation in *Drosophila*. *J. Neurobiol.* 14:207–225.

Kuromi, H., and Y. Kidokoro. 1998. Two distinct pools of synaptic vesicles in single presynaptic boutons in a temperature-sensitive *Drosophila* mutant, shibire. *Neuron.* 20:917–925.

Kuromi, H., and Y. Kidokoro. 2000. Tetanic stimulation recruits vesicles from reserve pool via a cAMP-mediated process in *Drosophila* synapses. *Neuron.* 27: 133–143.

Kuromi, H., and Y. Kidokoro. 2002. Selective replenishment of two vesicle pools depends on the source of $Ca^{2+}$ at the *Drosophila* synapse. *Neuron.* 35:333–343.

Lawe, D.C., V. Patki, R. Heller-Harrison, D. Lambright, and S. Corvera. 2000. The FYVE domain of early endosome antigen 1 is required for both phosphatidylinositol 3-phosphate and Rab5 binding. Critical role of this dual interaction for endosomal localization. *J. Biol. Chem.* 275:3699–3705.

Loewen, C.A., J.M. Mackler, and N.E. Reist. 2001. *Drosophila* synaptotagmin/null mutants survive to early adulthood. *Genesis.* 31:30–36.

Martin, A.R. 1955. A further study of the statistical composition of the end-plate potential. *J. Physiol.* 130:114–122.

Maycox, P.R., E. Link, A. Reetz, S.A. Morris, and R. Jahn. 1992. Clathrin-coated vesicles in nervous tissue are involved primarily in synaptic vesicle recycling. *J. Cell Biol.* 118:1379–1388.

McLauchlan, H., J. Newell, N. Morrice, A. Osborne, M. West, and E. Smythe. 1998. A novel role for Rab5-GDI in ligand sequestration into clathrin-coated pits. *Curr. Biol.* 8:34–45.

Mills, I.G., A.T. Jones, and M.J. Clague. 1998. Involvement of the endosomal autoantigen EEA1 in homotypic fusion of early endosomes. *Curr. Biol.* 8:881–884.

Misra, S., and J.H. Hurley. 1999. Crystal structure of a phosphatidylinositol 3-phosphate-specific membrane-targeting motif, the FYVE domain of Vps27p. *Cell.* 97:657–666.

Murthy, V.N., and C.F. Stevens. 1998. Synaptic vesicles retain their identity through the endocytic cycle. *Nature.* 392:497–501.

Neher, E., and R.S. Zucker. 1993. Multiple calcium-dependent processes related to secretion in bovine chromaffin cells. *Neuron.* 10:21–30.

Nielsen, E., S. Christoforidis, S. Uttenweiler-Joseph, M. Miaczynska, F. Dewitte, M. Wilm, B. Hoflack, and M. Zerial. 2000. Rabenosyn-5, a novel Rab5 effector, is complexed with hVPS45 and recruited to endosomes through a FYVE finger domain. *J. Cell Biol.* 151:601–612.

Nishikawa, K., and Y. Kidokoro. 1995. Junctional and extrajunctional glutamate receptor channels in *Drosophila* embryos and larvae. *J. Neurosci.* 15:7905–7915.

Novick, P., and M. Zerial. 1997. The diversity of Rab proteins in vesicle transport. *Curr. Opin. Cell Biol.* 9:496–504.

Olkkonen, V.M., and H. Stenmark. 1997. Role of Rab GTPases in membrane traffic. *Int. Rev. Cytol.* 176:1–85.

Osborne, S.L., J. Herreros, P.I. Bastiaens, and G. Schiavo. 1999. Calcium-dependent oligomerization of synaptotagmins I and II. Synaptotagmins I and II are localized on the same synaptic vesicle and heterodimerize in the presence of calcium. *J. Biol. Chem.* 274:59–66.

Pyle, J.L., E.T. Kavalali, E.S. Piedras-Renteria, and R.W. Tsien. 2000. Rapid reuse of readily releasable pool vesicles at hippocampal synapses. *Neuron.* 28:221–231.

Ramaswami, M., K.S. Krishnan, and R.B. Kelly. 1994. Intermediates in synaptic vesicle recycling revealed by optical imaging of *Drosophila* neuromuscular junctions. *Neuron.* 13:363–375.

Richards, D.A., C. Guatimosim, and W.J. Betz. 2000. Two endocytic recycling

Published May 12, 2003



routes selectively fill two vesicle pools in frog motor nerve terminals. *Neuron.* 27:551–559.

Ringstad, N., H. Gad, P. Low, G. Di Paolo, L. Brodin, O. Shupliakov, and P. De Camilli. 1999. Endophilin/SH3p4 is required for the transition from early to late stages in clathrin-mediated synaptic vesicle endocytosis. *Neuron.* 24: 143–154.

Roberts, R.L., M.A. Barbieri, K.M. Pryse, M. Chua, J.H. Morisaki, and P.D. Stahl. 1999. Endosome fusion in living cells overexpressing GFP-Rab5. *J. Cell Sci.* 112:3667–3675.

Roos, J., and R.B. Kelly. 1999. The endocytic machinery in nerve terminals surrounds sites of exocytosis. *Curr. Biol.* 9:1411–1414.

Ryan, T.A., and S.J. Smith. 1995. Vesicle pool mobilization during action potential firing at hippocampal synapses. *Neuron.* 14:983–989.

Sankaran, V.G., D.E. Klein, M.M. Sachdeva, and M.A. Lemmon. 2001. High-affinity binding of a FYVE domain to phosphatidylinositol 3-phosphate requires intact phospholipid but not FYVE domain oligomerization. *Biochemistry*. 40:8581–8587.

Schmidt, A., M. Wolde, C. Thiele, W. Fest, H. Kratzin, V. Podtelejnikov Alexandre, W. Witke, B. Huttner Wieland, and H.-D. Soeling. 1999. Endophilin I mediates synaptic vesicle formation by transfer of arachidonate to lysophosphatidic acid. *Nature.* 401:133–149.

Schuster, C.M., G.W. Davis, R.D. Fetter, and C.S. Goodman. 1996a. Genetic dissection of structural and functional components of synaptic plasticity. I. Fasciclin II controls synaptic stabilization and growth. *Neuron.* 17:641–654.

Schuster, C.M., G.W. Davis, R.D. Fetter, and C.S. Goodman. 1996b. Genetic dissection of structural and functional components of synaptic plasticity. II. Fasciclin II controls presynaptic structural plasticity. *Neuron.* 17:655–667.

Shupliakov, O., P. Low, D. Grabs, H. Gad, H. Chen, C. David, K. Takei, P. De Camilli, and L. Brodin. 1997. Synaptic vesicle endocytosis impaired by disruption of dynamin-SH3 domain interactions. *Science.* 276:259–263.

Simonsen, A., R. Lippe, S. Christoforidis, J.M. Gaullier, A. Brech, J. Callaghan, B.H. Toh, C. Murphy, M. Zerial, and H. Stenmark. 1998. EEA1 links PI(3)kinase function to Rab5 regulation of endosome fusion. *Nature.* 394: 494–498.

Sonnichsen, B., S. De Renzis, E. Nielsen, J. Rietdorf, and M. Zerial. 2000. Distinct membrane domains on endosomes in the recycling pathway visualized by multicolor imaging of Rab4, Rab5, and Rab11. *J. Cell Biol.* 149:901–914.

Stenmark, H., R.G. Parton, O. Steele-Mortimer, A. Luetcke, J. Gruenberg, and M. Zerial. 1994. Inhibition of rab5 GTPase activity stimulates membrane fusion in endocytosis. *EMBO J.* 13:1287–1296.

Stenmark, H., G. Vitale, O. Ullrich, and M. Zerial. 1995. Rabaptin-5 is a direct effector of the small GTPase Rab5 in endocytic membrane fusion. *Cell.* 83: 423–432.

Stevens, C.F., and J.H. Williams. 2000. "Kiss and run" exocytosis at hippocampal synapses. *Proc. Natl. Acad. Sci. USA.* 97:12828–12833.

Stewart, B.A., H.L. Atwood, J.J. Renger, J. Wang, and C.F. Wu. 1994. Improved stability of *Drosophila* larval neuromuscular preparations in haemolymph-like physiological solutions. *J. Comp. Physiol.* 175:179–191.

Sun, B., and P.M. Salvaterra. 1995. Two *Drosophila* nervous system antigens, Nervana 1 and 2, are homologous to the beta subunit of $Na^+$,$K^+$-ATPase. *Proc. Natl. Acad. Sci. USA.* 92:5396–5400.

Swanson, M.M., and C.A. Poodry. 1981. The *shibire*$^{ts}$ mutant of *Drosophila*: a probe for the study of embryonic development. *Dev. Biol.* 84:465–470.

Takei, K., P.S. McPherson, S.L. Schmid, and P. De Camilli. 1995. Tubular membrane invaginations coated by dynamin rings are induced by GTP-γS in nerve terminals. *Nature.* 374:186–190.

Takei, K., O. Mundigl, L. Danielle, and P. De Camilli. 1996. The synaptic vesicle cycle: a single vesicle budding step involving clathrin and dynamin. *J. Cell Biol.* 133:1237–1250.

Teng, H., and R.S. Wilkinson. 2000. Clathrin-mediated endocytosis near active zones in snake motor boutons. *J. Neurosci.* 20:7986–7993.

Valtorta, F., J. Meldolesi, and R. Fesce. 2001. Synaptic vesicles: is kissing a matter of competence? *Trends Cell Biol.* 11:324–328.

Wilson, J.M., M. de Hoop, N. Zorzi, B.H. Toh, C.G. Dotti, and R.G. Parton. 2000. EEA1, a tethering protein of the early sorting endosome, shows a polarized distribution in hippocampal neurons, epithelial cells, and fibroblasts. *Mol. Biol. Cell.* 11:2657–2671.

Wu, M.N., J.T. Littleton, M.A. Bhat, A. Prokop, and H.J. Bellen. 1998. ROP, the *Drosophila* Sec1 homolog, interacts with syntaxin and regulates neurotransmitter release in a dosage-dependent manner. *EMBO J.* 17:127–139.

Zenisek, D., J.A. Steyer, and W. Almers. 2000. Transport, capture and exocytosis of single synaptic vesicles at active zones. *Nature.* 406:849–854.

Zerial, M., and H. McBride. 2001. Rab proteins as membrane organizers. *Nat. Rev. Mol. Cell Biol.* 2:107–117.

Zhang, B., Y.H. Koh, R.B. Beckstead, V. Budnik, B. Ganetzky, and H.J. Bellen. 1998. Synaptic vesicle size and number are regulated by a clathrin adaptor protein required for endocytosis. *Neuron.* 21:1465–1475.

Zinsmaier, K.E., A. Hofbauer, G. Heimbeck, G.O. Pflugfelder, S. Buchner, and E. Buchner. 1990. A cysteine-string protein is expressed in retina and brain of *Drosophila*. *J. Neurogenet.* 7:15–29.